

CWRF performance at downscaling China climate characteristics

Xin-Zhong Liang^{1,2,3} · Chao Sun^{1,2} · Xiaohui Zheng^{2,4} · Yongjiu Dai⁵ · Min Xu⁶ · Hyun I. Choi⁷ · Tiejun Ling⁸ · Fengxue Qiao⁹ · Xianghui Kong¹⁰ · Xunqiang Bi¹⁰ · Lianchun Song¹¹ · Fang Wang¹¹

Received: 19 December 2017 / Accepted: 4 May 2018 © Springer-Verlag GmbH Germany, part of Springer Nature 2018

Abstract

The performance of the regional Climate-Weather Research and Forecasting model (CWRF) for downscaling China climate characteristics is evaluated using a 1980–2015 simulation at 30 km grid spacing driven by the ECMWF Interim reanalysis (ERI). It is shown that CWRF outperforms the popular Regional Climate Modeling system (RegCM4.6) in key features including monsoon rain bands, diurnal temperature ranges, surface winds, interannual precipitation and temperature anomalies, humidity couplings, and 95th percentile daily precipitation. Even compared with ERI, which assimilates surface observations, CWRF better represents the geographic distributions of seasonal mean climate and extreme precipitation. These results indicate that CWRF may significantly enhance China climate modeling capabilities.

 $\textbf{Keywords} \ \ Regional \ climate \ model \cdot Downscaling \ performance \cdot Extreme \ precipitation \cdot Diurnal \ temperature \ range \cdot Surface \ wind \cdot CWRF$

1 Introduction

Regional climate models (RCMs) are commonly used in high-resolution modeling for physical process understanding, seasonal climate prediction, climate change projection, and climate impact assessment (Giorgi 2006; Xue

Electronic supplementary material The online version of this article (https://doi.org/10.1007/s00382-018-4257-5) contains supplementary material, which is available to authorized users.

Published online: 21 May 2018

- Department of Atmospheric and Oceanic Science, University of Maryland, College Park, MD, USA
- Earth System Science Interdisciplinary Center, University of Maryland, 5825 University Research Court, Suite 4001, College Park, MD 20740, USA
- Climate, Environment and Sustainability Center, School of Atmospheric Science, Nanjing University of Information Science and Technology, Nanjing, China
- College of Global Change and Earth System Science, Beijing Normal University, Beijing, China
- School of Atmospheric Sciences, Sun Yat-Sen University, Guangzhou, China

et al. 2014; Giorgi and Gutowski 2015). Accordingly, over a dozen RCMs have been developed and evaluated, with the objective of adding value to the larger-scale driving features resolved by general circulation model (GCM) simulations or observational reanalyses. The skills and biases of various RCMs over major domains have been well documented in regional model intercomparison projects (Roads et al. 2003; Fu et al. 2005; Rinke et al. 2006; Christensen et al. 2007; Mearns et al. 2012; Nikulin et al. 2012). This

- ⁶ Climate Change Science Institute, Oak Ridge National Laboratory, Oak Ridge, TN, USA
- Department of Civil Engineering, Yeungnam University, Gyeongsan, South Korea
- Key Laboratory of Research on Marine Hazards Forecasting, National Marine Environmental Forecasting Center, Beijing, China
- ⁹ Key Laboratory of Geographic Information Science, Ministry of Education, East China Normal University, Shanghai, China
- Olimate Change Research Center, Institute of Atmospheric Physics, Chinese Academy of Sciences, Beijing, China
- National Climate Center, China Meteorological Administration, Beijing, China



study documents the performance of the Climate-Weather Research and Forecasting model (CWRF, Liang et al. 2012) over China.

Twelve major RCMs, some with multiple variants, are typically used for regional climate modeling over China or East Asia. Their relevant applications are summarized in Table 1, including model resolutions, integration periods, study focuses, and references. [All RCM acronyms and other key abbreviations are listed in "Appendix A".] Seven of these models participated in the East Asian Regional Model Intercomparison Project (RMIP), which compared present performance and future projections given identical driving conditions from a GCM simulation or reanalysis (Fu et al. 2005). These include GRIMs, JSM, MM5, RAMS, RegCM, RIEMS, and WRF (Feng and Fu 2006; Feng et al. 2011; Niu et al. 2015; Li et al. 2016; Tang et al. 2016; Wu et al. 2016). RSM was compared with WRF and RegCM for past climate performance (Wang et al. 2015), PRECIS, CCLM, and LMDZ were individually evaluated in both the present and future climate conditions, and IPRC was tested only in a summer case study.

The most popular of these models is RegCM, which is based on MM5 (Grell et al. 1994) and evolved from version 2 (Giorgi et al. 1993a, b) to version 3 (Pal et al. 2007) to the current version 4 (Giorgi et al. 2012). All three versions have been used for climate studies over the region (see Table 1 for the references), including sensitivities to model configurations such as lateral/initial conditions and horizontal/vertical resolutions; effects of terrain details, land use changes, land/ocean-atmospheric interactions, and cumulus parameterization and other physics improvements; and climate projections driven by various GCMs. These studies showed a large range of RegCM-simulated present climate biases and future trend uncertainties.

Recently, WRF has been increasingly used as an RCM for China or East Asian climate modeling. Some studies have examined its added value for downscaling GCM simulations (Yu et al. 2010) and reanalyses (Sato and Xue 2013; Gao et al. 2015), as well as its performance sensitivity to driving lateral conditions (Yang et al. 2012) and land surface representations (Li et al. 2015). Others have evaluated its ability to hindcast seasonal climate anomalies (Yuan et al. 2012; Ma et al. 2015) and project future climate changes, focusing on extreme events (Yu et al. 2015; Bao et al. 2015). Wang et al. (2015) compared the performance of WRF with RegCM4 and RSM in simulating China precipitation and temperature interannual variations, linear trends and extreme events during 1989-2008. Their results showed substantial differences in regional climate biases between the models, none of which had significantly superior skill.

WRF was designed originally for short-range numerical weather prediction but not expressly for long-term climate simulation. Liang et al. (2012) noted that direct climate

applications of WRF are limited by its inadequate representation of essential physics at relevant scales, and therefore developed its climate extension CWRF with crucial improvements to land–atmosphere–ocean, convection–microphysics, and cloud–aerosol–radiation interactions, as well as system consistency throughout all process modules. As a result, CWRF more realistically simulates surface radiation, terrestrial hydrology, and precipitation (Choi and Liang 2010; Yuan and Liang 2011a; Liang et al. 2012; Liang and Zhang 2013; Qiao and Liang 2015, 2016a, b), and improves WRF regional climate prediction in the United States (Yuan and Liang 2011b; Liang et al. 2012; Liu et al. 2016; Chen et al. 2016). This study evaluates CWRF simulation of China climate characteristics during 1980–2015, relative to the latest RegCM4.6 simulations.

2 Model description

CWRF has been continuously developed since 2002 as a Climate extension of WRF (Skamarock et al. 2008) through improvements to the representation of numerous physical processes and integration of external (top, surface, lateral) forcings crucial to climate scales (Liang et al. 2012). It couples a state-of-the-art Conjunctive Surface-Subsurface Process model (CSSP) to predict detailed terrestrial hydrology and land-atmosphere interaction. CSSP is rooted in the Common Land Model (CoLM, Dai et al. 2003, 2004), with updates from the Community Land Model (CLM, Oleson et al. 2013). It integrates vertical water exchange (precipitation, evaporation, transpiration, infiltration) and hydraulic redistribution by deep vegetation roots; it also represents horizontal water movement (across grids) as surface and subsurface runoff resulting from rainfall excess and saturation depletion, as well as lateral flows due to resolved and subgrid topographic controls (Choi et al. 2007, 2013; Choi and Liang 2010; Yuan and Liang 2011a). It incorporates realistic distributions of surface (soil and vegetation) characteristics (Liang et al. 2005a) and an advanced dynamicstatistical parameterization of land surface albedo (Liang et al. 2005b) to enable credible evaluation of land use/land cover effects on regional climate (Xu et al. 2014). CWRF also couples a comprehensive multi-level upper ocean model (UOM, Ling et al. 2011, 2015) to resolve transient air-sea interactions critical to sea surface temperature diurnal cycle and daily variations, as well as a detailed Lake, Ice, Snow, and Sediment Simulator (LISSS, Subin et al. 2012) to predict the thermal effects of freshwater lake interactions with the atmosphere.

Furthermore, CWRF integrates a comprehensive ensemble of alternate parameterization schemes for each of the key physical processes, including surface (land, ocean), planetary boundary layer, cumulus (deep, shallow), microphysics,



Table 1 Summary of 12 RCMs used for regional climate modeling over China or East Asia, including model resolution (horizontal grid size: km; vertical level number: L), integration period (longest combined: ∼ else: -), study focus, and references

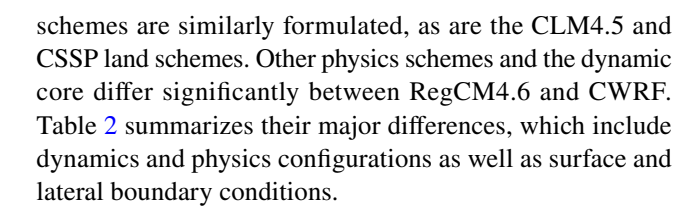
) reaginar)	(rongest combined: " cisc. "), study tocus, and references	ocus, and ichemes		
RCM	Resolution	Period	Focus	References
CCLM	(14, 50) km; 40 L	1979–2100 1961–2000, 2011–2050	Evaluation, projection	Fischer et al. (2013), Wang et al. (2013), Bucchignani et al. (2014)
GRIMs	50 km; 28 L	1978-2000, 2041-2070 1980-2050 Evaluation, projection RMIP	Evaluation, projection RMIP	Lee et al. (2014), Niu et al. (2015), Li et al. (2016), Tang et al. (2016), Wu et al. (2016)
IPRC	55 km; 28 L	1998	Flooding case	Wang et al. (2003)
JSM	60 km; 23 L	1988–1998	Evaluation	Feng and Fu (2006), Feng et al. (2011)
LMDZ	50–66 km; 19 L	1961–2005 1961–1990, 2041–2050	Evaluation, projection	Zou et al. (2010), Chen et al. (2011), Yang et al. (2016)
MM5	(50, 60) km; 23 L	1979–2006 1981–2000, 2041–2060 1978–2000, 2038–2070	Evaluation, projection air-sea interaction RMIP	Kang et al. (2005), Feng and Fu (2006), Feng et al. (2011), Hu et al. (2013), Cha et al. (2016), Li et al. (2016), Tang et al. (2016)
RAMS	50 km	1981–2000, 2041–2060	Projection; RMIP	Li et al. (2016), Tang et al. (2016)
RegCM	v2 45–360 km (14, 16, 20) L	1986–1998	Sensitivity to resolution, physics, terrain, land use; RMIP	Gao et al. (2001, 2002, 2003, 2006), Chan et al. (2004), Feng and Fu (2006), Chow et al. (2008), Feng et al. (2011)
	v3 15–90 km (14, 18, 23)L	1982–2007 1980–2005, 2015–2040 1990–1999, 2046–2055 1981–2000, 2041–2060 1980–2000, 2010–2098 1961–1990, 2071–2100	Sensitivity to resolution, cumulus scheme, LBCs, SBCs, air-sea interaction evaluation, projection; RMIP	Gao et al. (2008, 2011, 2012), Liu et al. (2009, 2011, 2013), Shi et al. (2009), Zou and Zhou (2011, 2013a, b), Marcella and Eltahir (2012), Huang et al. (2013), Hui et al. (2014), Zou et al. (2014, 2016), Li et al. (2016), Tang et al. (2016), Wu et al. (2016), Zeng et al. (2016)
	v4 (25, 30, 50) km; 18 L	1986–2005, 2031–2050 1970–2005, 2070–2099 1981–2050, 1950–2099	Sensitivity to cumulus, land-air interaction; evaluation, projection	Gu et al. (2012), Gao et al. (2013, 2016), Liu et al. (2014), Oh et al. (2014), Ji and Kang (2015), Wang et al. (2015), Wu et al. (2015)
RIEMS	(50, 60) km 17 L	1979–2008	Air-sea interaction; evaluation; RMIP	Feng and Fu (2006), Feng et al. (2011), Zhao (2012, 2013), Fang et al. (2013)
RSM	(30, 60) km; 28 L	1989–2008	Cumulus; evaluation	Kang and Hong (2008), Wang et al. (2015)
PRECIS	(25, 50) km; 19 L	1961–1990, 2071–2100 1981– 2050; 1950–2099	Evaluation, projection	Zhang et al. (2006), Wu et al. (2015), Guo et al. (2017)
WRF	(30, 50, 60) km 26 L	1978–2012 1976–2005, 2031–2050 1978–2000, 2041–2070 1981–2000, 2041–2060 2052–2070, 1946–2100	Land surface schemes seasonal prediction evaluation, projection RMIP	Yu et al. (2010, 2015), Yang et al. (2012), Yuan et al. (2012), Sato and Xue (2013), Bao et al. (2015), Gao et al. (2015), Li et al. (2015, 2016), Ma et al. (2015), Wang et al. (2015), Tang et al. (2016), Wu et al. (2016)



cloud, aerosol, and radiation (Liang et al. 2012). This facilitates the use of an optimized physics ensemble approach to improve weather or climate prediction (Liang et al. 2007, 2012; Zeng et al. 2008; Liu et al. 2009; Yuan et al. 2012) while providing reliable uncertainty estimates. In particular, CWRF has a built-in Cloud-Aerosol-Radiation (CAR) ensemble model that incorporates a wide variety of alternate parameterizations for cloud properties (cover, water, radius, optics, geometry), aerosol properties (type, profile, optics), radiation transfers (solar, infrared), and their interactions (Liang and Zhang 2013). CAR enables full quantification of radiative forcings and climate impacts as well as their uncertainties, all of which strongly depend on the choice of cloud, aerosol and radiation schemes (Zhang et al. 2013). CWRF also has a built-in ensemble cumulus parameterization (ECP), which uses a suite of alternate closure assumptions that may drastically affect rainfall distribution, frequency and intensity, and diurnal cycle (Liang et al. 2004a; Qiao and Liang 2015, 2016a, b). The optimized ECP ensemble can significantly improve precipitation prediction.

This study uses the following CWRF physics configuration as the control version: Cumulus—ECP penetrative convection (Qiao and Liang 2016a, b) plus UW shallow convection (Bretherton and Park 2009), Microphysics—GSFCGCE (Tao et al. 2003), Cloud—XRL (Xu and Randall 1996; Liang et al. 2004b), *Aerosol*—MISR (Kahn et al. 2005, 2007; Zhao et al. 2009), Radiation—GSFCLXZ (Chou and Suarez 1999; Chou et al. 2001), Planetary Boundary Layer (PBL)—CAM (improved Holtslag and Boville 1993) plus ORO (Rontu 2006; Liang et al. 2006), and Surface—CSSP land plus UOM ocean (described above). A more detailed description of these schemes is provided in Liang et al. (2012), with the key differences in the ECP, CSSP, and UOM updates referenced above. For each new regional domain, CWRF must be carefully localized to maximize its performance. In addition to these physics improvements, the CWRF localization for this study region includes the specific domain design and construction of surface boundary conditions (see Sect. 3). In particular, the dynamic surface albedo parameterization (Liang et al. 2005b) must be re-developed according to the updated vegetation data (Xu et al. 2014), and stream flow directions must be re-constructed (Choi et al. 2013) with visual reality check, both of which are time consuming and labor intensive.

RegCM4.6 (Giorgi et al. 2012) has been continuously developed from MM5 (Grell et al. 1994) over the last three decades. The physics configuration chosen for the present study includes *Cumulus*—TDK penetrative plus shallow convection (Tiedtke 1989), *Microphysics*—SUBEX (Pal et al. 2000), *Cloud+Radiation*—CCM3 (Kiehl et al. 1996), *PBL*—CCM3 (Holtslag et al. 1990), and *Surface*—CLM4.5 land processes (Oleson et al. 2013) plus surface fluxes over oceans (Zeng et al. 1998). The CCM3 and CAM PBL



3 Model experiment design and observational reference data

The CWRF computational domain in this study (Fig. 1) is based on the Lambert conformal map projection centered at (35.18°N, 110°E) with a total of 232×172 grid points at 30 km spacing. Liu et al. (2008) demonstrated that this domain is optimal for modeling China's regional climate, which is determined by interactions between the planetary circulation (as forced by lateral boundary conditions or LBCs) and East Asian surface processes, including orography, soil, vegetation and coastal oceans. Figure 1 depicts a small subset of the comprehensive surface boundary conditions (SBCs) used by CWRF (Liang et al. 2005a; Xu et al. 2014), showing the land cover and ocean depth distributions, lakes, major rivers, and main streams. In the buffer zones, located across 14 grids along the four edges of the domain, varying LBCs were specified using a dynamic relaxation technique with linear-exponential nudging coefficients that decrease toward the surface and the inner boundaries (Liang et al. 2001). By default, CWRF uses 36 terrain-following vertical levels with the upper boundary at 5distributions over Mainland0 hPa (Liang et al. 2012). Both the horizontal and vertical resolutions for CWRF are relatively finer than most RCMs applied for long-term simulations in the region, which typically use ~ 50 km grids and ~ 20 levels.

RegCM4.6 uses the same domain (Fig. 1), but includes only 9 grids in the buffer zones with exponential nudging coefficients (Giorgi et al. 1993b). It uses relatively stronger (especially near the surface) and faster (toward the inner domain) relaxation than does CWRF (Liang et al. 2001). As typically applied, the model has only 18 vertical levels, half that of CWRF, with the same 50 hPa upper boundary. As designated for its interactive CLM4.5 (Oleson et al. 2013), RegCM4.6 employs 7 primary plant function types, whose properties (such as leaf and stem area indices) are derived from IGBP and other satellite data (Bonan et al. 2002). These land use/cover specifications differ from those of CWRF/CSSP, which incorporates USGS's 24 dominant categories and MODIS satellite data (Liang et al. 2005a, b; Xu et al. 2014).

Both CWRF and RegCM4.6 simulations were driven by the ECMWF Interim reanalysis (ERI, Dee et al. 2011), one of the best available proxies for observations. They were initiated on October 1, 1979 and integrated continuously



Table 2 Summary of major differences between CWRF and RegCM4.6 configurations

	CWRF	RegCM4.6
Dynamics configuration		
Dynamic core	Non-hydrostatic WRF	Hydrostatic MM5
Vertical levels	36	18
Lateral boundary conditions		
Buffer zones	14 grids	9 grids
Dynamic relaxation	Linear-exponential nudging coefficients (Liang et al. 2001)	Exponential nudging coefficients (Giorgi et al. 1993b)
Surface boundary conditions		
Land	USGS 24 dominant categories (Liang et al. 2005a; Xu et al. 2014)	MODIS 20 categories with hierarchy plant functional types (Lawrence 2007)
Physics configuration		
Cumulus	ECP penetrative convection (Qiao and Liang 2016a,b) plus UW shallow convection (Bretherton and Park 2009)	TDK penetrative plus shallow convection (Tiedtke 1989)
Microphysics	GSFCGCE (Tao et al. 2003)	SUBEX (Pal et al. 2000)
Cloud	XRL (Xu and Randall 1996; Liang et al. 2004b)	CCM3 (Kiehl et al. 1996)
Aerosol	MISR (Kahn et al. 2005, 2007; Zhao et al. 2009)	None
Radiation	GSFCLXZ (Chou and Suarez 1999; Chou et al. 2001)	CCM3 (Kiehl et al. 1996)
PBL	CAM (improved Holtslag and Boville 1993) plus ORO (Rontu 2006; Liang et al. 2006)	CCM3 (Holtslag et al. 1990)
Surface		
Land	CoLM-CSSP conjunctive surface–subsurface physical and hydrological processes (Choi 2007,2013; Liang et al. 2005a, b)	CLM4.5 land processes (Oleson et al. 2013)
Ocean	UOM upper ocean with transient air-sea interactions (Ling et al. 2011, 2015)	Prescribed SST daily variations

through December 31, 2015. The first two months are considered spin-up and were not used in the subsequent analyses. Sea surface temperature (SST) was prescribed from the daily observational analysis, available over the global oceans on a ¼° longitude by latitude grid mesh from November 1981 onward (Reynolds et al. 2007; Banzon et al. 2016). Before that, SST was supplemented by ERI daily mean ground temperature. For CWRF, the daily SST analysis was used as relaxation in UOM to predict ocean temperature variations (including the diurnal cycle) due to transient airsea interactions (Ling et al. 2011, 2015). On the other hand, SST in RegCM4.6 varies exactly according to the prescribed daily means.

As the reference for model evaluation, observational data consist of a gridded (¼° longitude by latitude) daily analysis of precipitation, surface air (2 m) temperature and humidity, and surface (10 m) wind based on in situ measurements at 2416 stations in Mainland China from 1961 onward (Wu and Gao 2013). Given China's total area of ~9.634M km², these stations, if evenly distributed, would each cover an equivalent 63 km grid, coarser than the ¼° analysis grid. However, the stations (principal plus ordinary) are sparse in western China (Fig. S1), including the Tibetan Plateau and the Taklamakan-Gobi Desert, where the analysis contains

substantial uncertainties due to arbitrary extrapolation from missing data. On the other hand, the stations are relatively dense in eastern China (east of ~100°E, except for the northern border including Inner Mongolia-Heilong Jiang), where the analysis represents climate characteristics at a finer resolution than the ERI ~80 km grid but still coarser than the CWRF 30 km grid. Consequently, our model evaluation focuses more on eastern China. Given different classifications of major climate regimes (Zheng et al. 2013; Shi et al. 2014; Han and Zhai 2015) and considering topographic characteristics and data availability, we further divide Mainland China into 11 broad regions (Fig. S1 provides names and boundaries) to evaluate regional model performance.

ERI uses a 4D-Var analysis to assimilate satelliteretrieved total column water vapor as a pseudo-observation of rainfall, as well as a separate surface analysis of screenlevel temperature and humidity synoptic observations, along with station snow depth and satellite snow cover data (Dee et al. 2011). As such, precipitation and surface air temperature data from ERI are among the most realistic proxies of observations over East Asia (Zhu et al. 2016; Huang et al. 2016). Downscaling RCMs do not directly assimilate surface measurements, but predict these variables as driven only by planetary circulation, especially upper air conditions (Liang



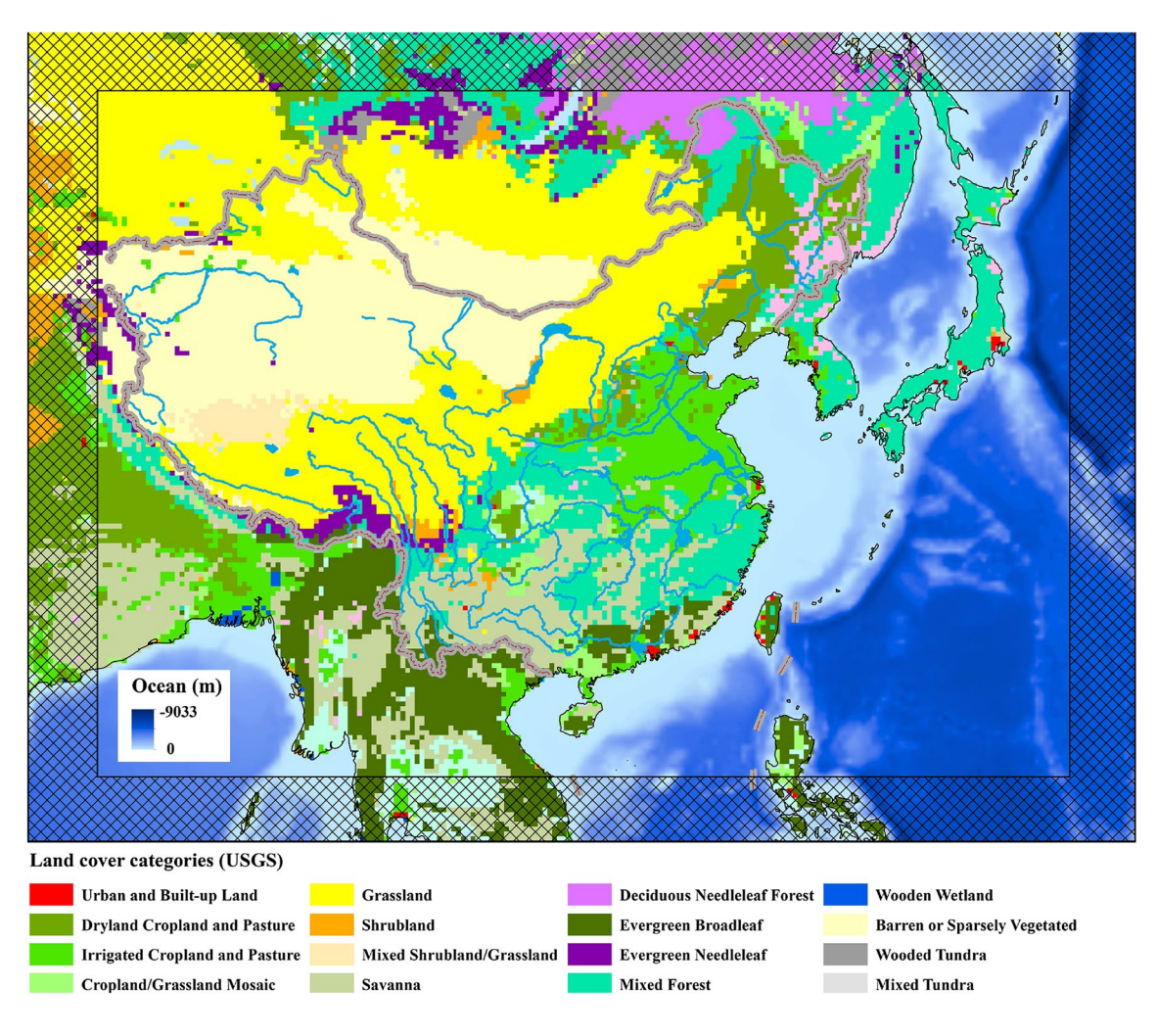


Fig. 1 The CWRF computational domain for this study, overlaid with land cover, ocean depth (m), lakes, major rivers, and main streams. The hatched edge areas are the buffer zones, where LBCs are specified

et al. 2001). Therefore, for RCMs to reproduce these variables with skill close to that of ERI is a significant achievement, not a general expectation. However, ERI uses measurements from significantly fewer than the 2416 stations used in Wu and Gao (2013), and thus cannot resolve the full characteristics in the reference data. As a result, RCMs may outperform ERI in certain circumstances, which would indicate that they incorporate more realistic physics representations (especially surface-atmosphere interactions) than ERI at this scale.

4 Annual cycle

Figure 2 uses a Taylor (2001) diagram to summarize the overall performances (relative to the driving ERI) of CWRF and RegCM4.6 in simulating seasonal mean precipitation geographic distributions over Mainland China. Spatial pattern correlations and normalized standard deviations are

compared with observations for all four seasonal means averaged during 1980–2015. To better describe precipitation characteristics, we include statistics for seasonal average amount, number of rainy days (> 0.1 mm), and simple daily intensity index (total accumulated amount / number of rainy days).

For precipitation amount, ERI strongly correlates to observed patterns, with some seasonal variation (0.77–0.82). It generally overestimates spatial variability (1.1–1.37), especially in autumn and summer, with winter closest to observations. In comparison, CWRF correlates less in summer (0.74), similarly in autumn (0.78), and more strongly in winter and spring (0.87), and even more significantly overestimates spatial variability (1.43–1.69). This increased variability may arise from the inability of the coarsely-resolved reference data to represent the actual signal. In contrast, the RegCM4.6 performs significantly worse, with lower correlations ranging from 0.42 (winter), 0.54 (autumn, summer) to 0.66 (spring).



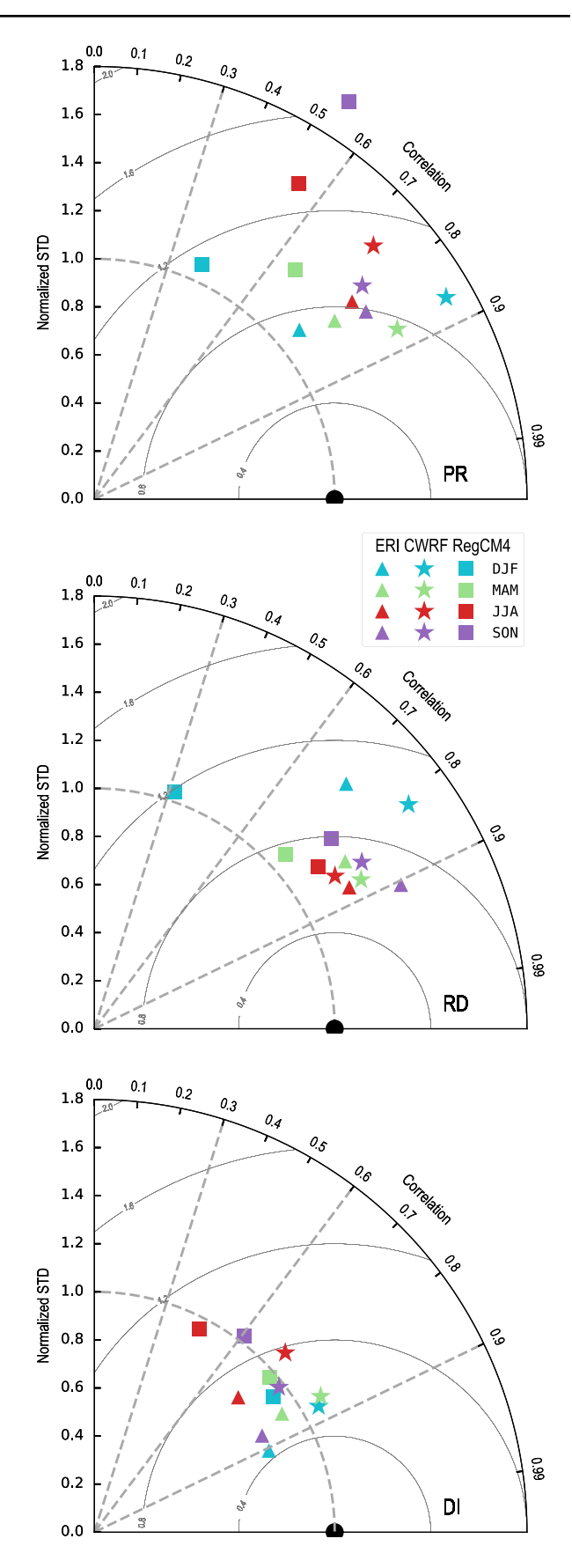
Fig. 2 Taylor diagram of pattern statistics in Mainland China comparing CWRF, RegCM4.6, and ERI overall performance in simulating geographic distributions of seasonal average precipitation amount (PR), number of rainy days (RD), and daily rainfall intensity (DI). Shown are the pattern correlation (azimuthal) and normalized standard deviations (radius) compared with observations. The dot marks the perfect score with a unit correlation and deviation

For the number of rainy days as compared with the precipitation amount, ERI correlates more highly to observed patterns (0.83–0.91) except in winter (0.71), and also overestimates spatial variability more significantly (1.35–1.46) except in summer (1.21). Likewise, CWRF correlates more strongly in summer and autumn (0.85), similarly in spring (0.87) and less in winter (0.81), while systematically reducing overestimation of spatial variability, especially in summer (1.19). As such, overall CWRF performs close to ERI. RegCM4.6 generally captures rainy days better than precipitation amount, with an increased correlation (0.74–0.81) except in winter (0.32), and its overestimation of variability is reduced (1.04–1.26). However, it is still outperformed by CWRF, especially in pattern correlation.

For daily rainfall intensity as compared with the other two measures, the main performance difference is that all models more realistically simulate spatial variability. In particular, CWRF produces standard deviations close to observations (0.98–1.10), which is an improvement over ERI's general underestimation (0.80–0.92). RegCM4.6 also simulates realistic variability (0.93–1.03), but has a systematically lower pattern correlation than CWRF and ERI for all seasons.

Figures 3 and 4 compare geographic distributions of the seasonal average precipitation amount and daily intensity. As discussed earlier, ERI assimilates pseudo-observations and station measurements and thus can well reproduce the general pattern and magnitude of precipitation in all seasons. In summer, the observed monsoon system consists of two major rain bands east of ~105°E: along the Yangtze River and across South China. ERI simulates a smoother structure, without a well-defined separating dry zone. In contrast, CWRF reproduces the two bands with a finer structure, but overestimates rainfall amount in South China, mainly by inflating the number of rainy days (Fig. S2). CWRF more realistically simulates daily intensity than ERI, which systematically underestimates both bands. Therefore, ERI produces a reasonable total amount by compensating for weaker intensity with more rainy days, a "drizzling problem" typical in GCMs (Sun et al. 2006). On the other hand, RegCM4.6 poorly simulates the two rain bands, with little organized structure and more scattered grid-point storms.

Another key summer feature is the moderate precipitation in the Northeast, which is strongest along the three mountain ridges surrounding the Northeast Plain (Da and Xiao Hinggan Liang, and Changbai Shan). ERI captures this well, in part due to its data assimilation. In contrast,





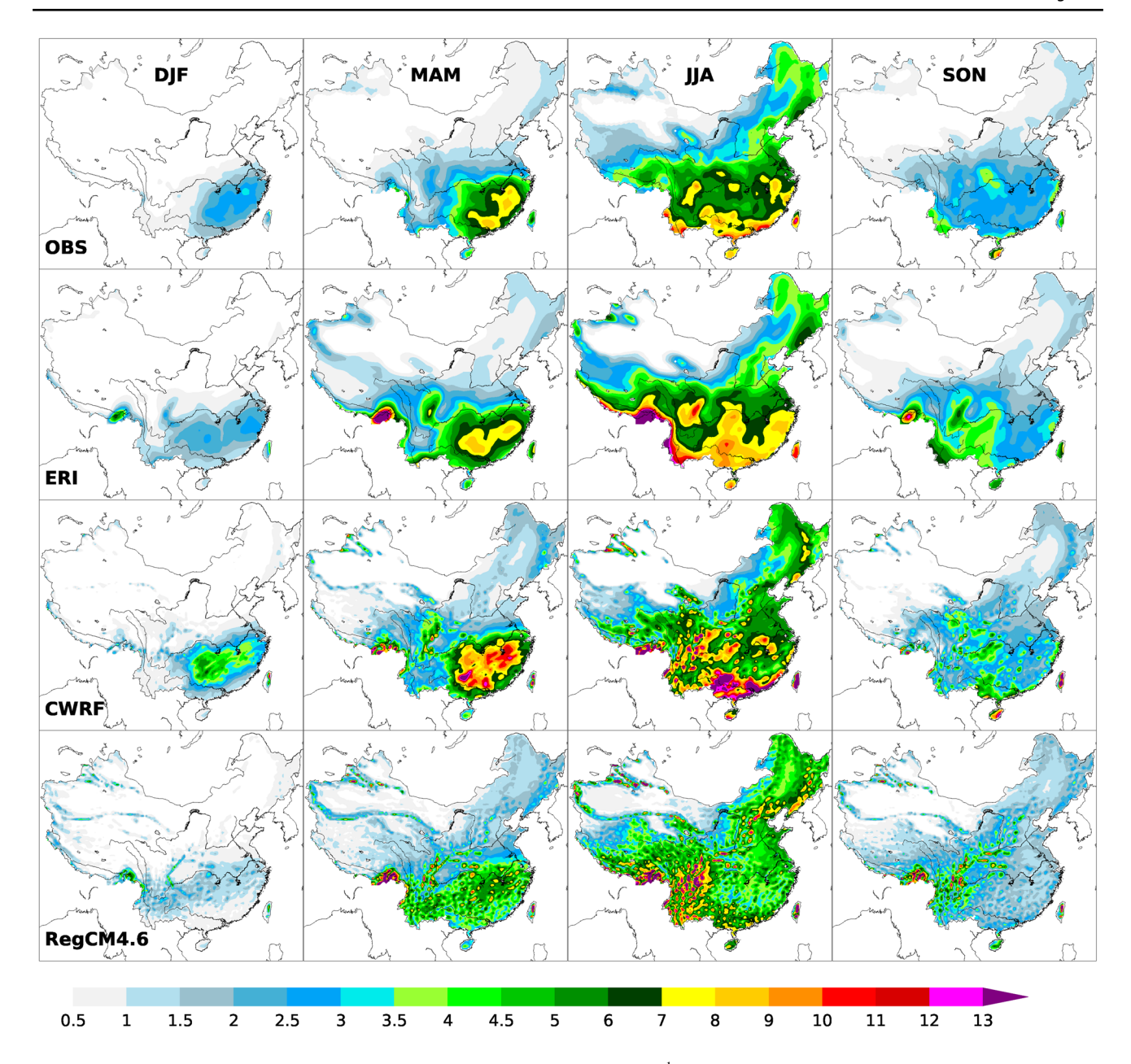


Fig. 3 Geographic distributions of seasonal average precipitation amount (mm day^{-1}) observed (OBS), assimilated (ERI), and downscaled by CWRF and RegCM4.6 for winter (DJF), spring (MAM), summer (JJA), and autumn (SON)

CWRF overpredicts the total amount and daily intensity but produces rainy days comparable to ERI. However, since monitoring stations over these mountains are sparse and mostly located at lower elevations, the reference data likely underestimate precipitation amount and intensity over mountains (Liang et al. 2004b). A finer-resolution monitoring network together with an objective topographic adjustment (Daly et al. 1994) is needed to provide more realistic reference data, against which model performance can be better evaluated.

Spring is China's second most essential precipitation season, with main rainfall occurring between the Yangtze

and Pearl Rivers. Observations exhibit two rainfall centers: immediate south of the Yangtze River and north of the Pearl River. ERI and CWRF both capture these centers, but ERI underestimates their intensity while CWRF overestimates it. On the other hand, RegCM4.6 fails to distinguish the two organized centers at all, producing scattered precipitation over the entire region. Again, the reference data may be inadequate to resolve topographic enhancement over this region, where numerous mountains have elevations exceeding 1 km.

Winter is China's dry monsoon season, with observed precipitation typically under 10 mm per day. Precipitation



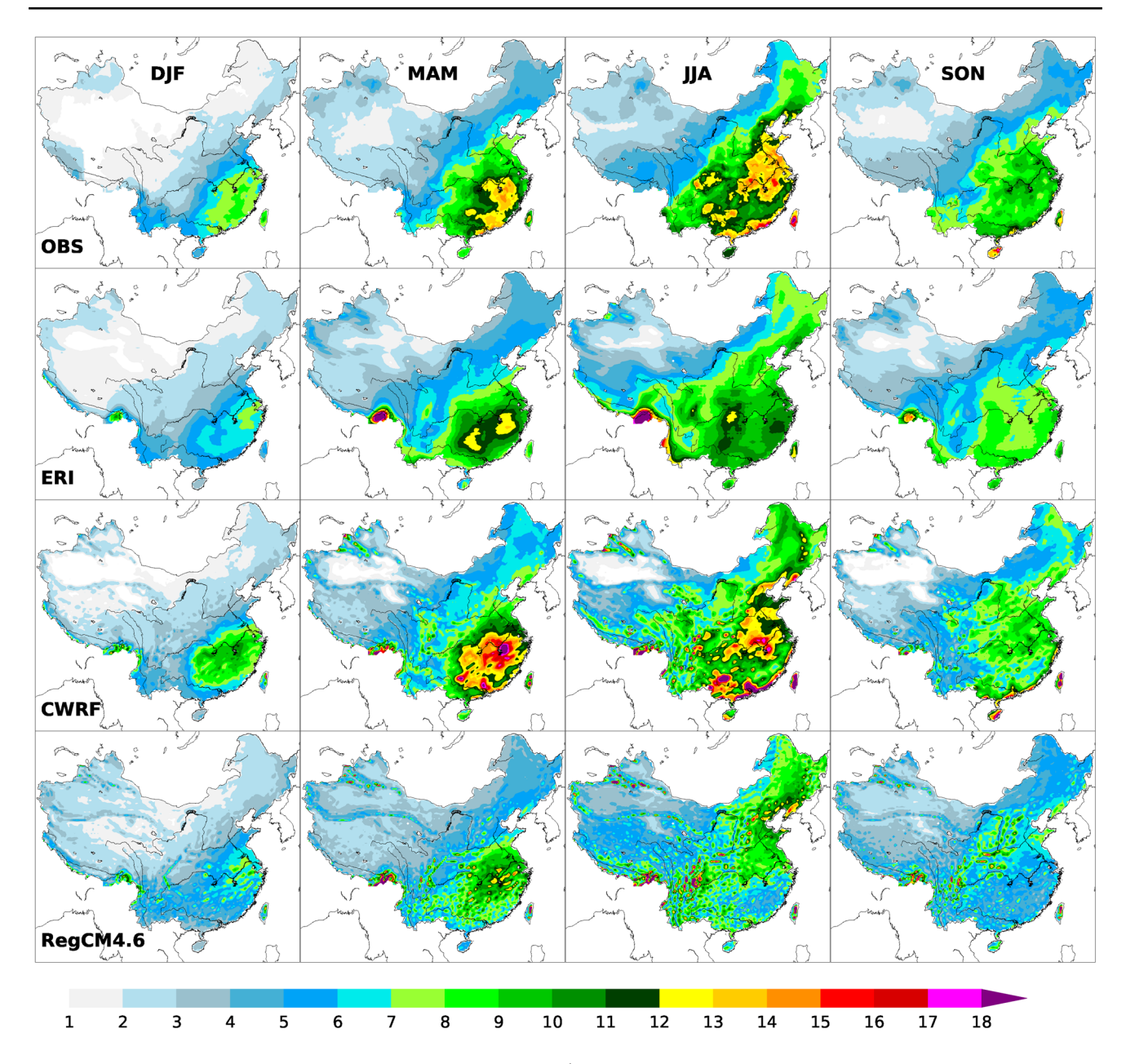


Fig. 4 Same as Fig. 3 except for seasonal mean daily intensity (mm day⁻¹)

is evenly distributed between the Pearl and Yangtze Rivers east of ~105°E. Model simulation of daily intensity is reasonable, with small underestimation by ERI and overestimation by CWRF, but less spatial correspondence by RegCM4.6. Biases are larger in rainy days, with ERI close to observations, CWRF overestimation (excessive amount) in the western part, and RegCM4.6 underestimation (deficit amount) in the eastern part. Since winter precipitation results primarily from non-convective systems, interactions among surface, PBL, and cloud microphysics parameterizations must be improved for models to more realistically capture rainy days.

Autumn is the transition season for China's summer to winter monsoon, with the main rainfall retreating west of ~110°E. East of that longitude, precipitation is fairly uniform (similar to winter but with broader coverage) except for enhancement along the southeastern coast where intensity is 10 mm day⁻¹ or higher. A weaker intensity center is observed over the Yangtze River Basin. These features are well captured by both CWRF and ERI, with some underestimation by the latter. In contrast, RegCM4.6 shifts the center over the Yangtze River Basin westward to the upper reach.

Notably, the reference data shows frequent rainfall in the southern foothills of the Yungui and Tibetan Plateaus,



especially in summer and spring, with moderate rainfall (~10 mm day⁻¹) on 75% of summer days. ERI captures this feature well, though it increases both intensity and coverage. Both CWRF and RegCM4.6 also reproduce the feature, but with a more scattered structure. Again, these areas contain sparse monitoring stations and hence little observational reference. The topographic uplifting effect on the prevailing moist southerly flow causes frequent rainfall, likely with heavier intensity than in the reference data, and the complex characteristics of the clustered mountains may lead to a more scattered rainfall structure. Thus, the CWRF or RegCM4.6 results may actually be more reasonable than the reference data.

For surface air temperature, the magnitude of spatial variations is much greater than that of model differences. Therefore, the spatial pattern correlations are all above 0.96 throughout the year. This applies to daily mean, maximum, and minimum, indicating that comparing these full temperature fields does not effectively separate model skill differences. Rather we compare their biases (simulations minus observations), including seasonal geographic maps and frequency distributions over Mainland China. Given that histograms are not smooth and depend on the width and end points of the bins, we use kernel density estimators to depict the frequency distributions (Hwang et al. 1994). This applies to all frequency distribution results presented below.

For the daily mean (Fig. 5), the bias frequency shows that ERI has a narrow peak around 1 °C, while RegCM4.6 has a widespread flattened pattern. The CWRF pattern is close to that of ERI, especially for the warm tail, indicating that it performs better overall than RegCM4.6. Important regional differences exist. ERI biases vary generally within ± 3 °C and mostly between ± 2 °C in all seasons, except for autumn, which is systematically 1-3 °C warmer. The ERI performance results from its surface data assimilation. In contrast, CWRF biases are comparable with or even smaller than ERI over broad regions in eastern China, where surface monitoring stations are relatively dense. This is most obvious to the south of the Yangtze River from spring to autumn. Exceptions include systematic colder biases in the Tibetan Plateau during winter and spring, and warmer biases in the Taklamakan-Gobi Desert during summer. The reference over these regions, however, is based on subjective extrapolation from measurements at a very limited number of stations, and so contains substantial uncertainties. RegCM4.6 produces similar biases in these regions. A more realistic reference is required to determine whether the biases are due to model errors or data uncertainties. In other regions, RegCM4.6 generates stronger warm biases than CWRF for all seasons, except for colder biases in North China spring.

For the daily maximum (Fig. S3), the bias frequency shows that ERI has a sharp peak around -1 °C (colder), RegCM4.6 again has a flatter pattern (here even further

widened), and the CWRF distribution is intermediate. ERI biases are systematically reduced relative to the daily mean, causing an improvement in most of eastern China and a skill loss to the west throughout the year. In winter and spring, ERI and CWRF both have consistent western cold biases; RegCM4.6 significantly enhances these cold biases, and generates them in most of northern China, suggesting enlarged daytime surface radiation deficits. In eastern China, CWRF performs well, with small biases mostly within ± 2 °C in both seasons, whereas RegCM4.6 produces much larger warm biases (3–7 °C in winter and 1–4 °C in spring) to the south of the Yangtze River and cold biases (2-6 °C in winter and 2-8 °C in spring) to the north of the Yellow River. RegCM4.6 may insufficiently represent snow and precipitation processes, since its performance improves (over the daily mean) in summer and autumn. In these seasons, ERI and CWRF are realistic across most of eastern China, as is RegCM4.6 to the north of the Yellow River. Exceptions include cold biases (1-3 °C) in summer for CWRF in the Pearl River Basin, and warm biases (2-5 °C) for RegCM4.6 in summer between the Yellow and Yangtze Rivers and in autumn between the Yellow and Pearl Rivers. These biases are opposite to precipitation biases shown in Fig. 3.

For the daily minimum (Fig. S4), the bias frequency shows that ERI peaks around 1 °C in autumn-winter and 2 °C in spring-summer, indicating an overall overestimation, whereas CWRF peaks near 0 °C with a flatter distribution, which is similar to but less skewed than RegCM4.6. ERI generates systematic warm biases (1-4 °C) over most of China, especially in spring and summer. CWRF also displays warm biases of similar magnitude, but these are generally limited to areas with sparse monitoring stations, in northern China in summer and autumn, and even further north in winter and spring. It produces cold biases over the Tibetan Plateau in winter and spring, with magnitudes similar to the daily mean and maximum biases. CWRF performs excellently across the rest of eastern China throughout the year. RegCM4.6 performance generally resembles CWRF, except that the summer and autumn warm biases are enhanced and expanded into North China, and spring cold biases (1–3 °C) occur broadly over the Northeast.

For the daily temperature range (maximum minus minimum, Fig. 6), ERI gives systematic underestimates, where the bias frequency peaks at -2 to -3 °C throughout the year. CWRF yields a general improvement, shifting the peaks to near -1 °C, albeit with a wider spread. RegCM4.6 produces a bimodal pattern, most obvious in winter, autumn, and spring, indicating that it enhances both negative and positive biases relative to CWRF. Even assimilating 6-hourly surface data analysis, ERI is still not able to accurately resolve the diurnal range. In contrast, CWRF, which incorporates only synoptic conditions above the boundary layer, successfully captures the diurnal range, especially in eastern China where



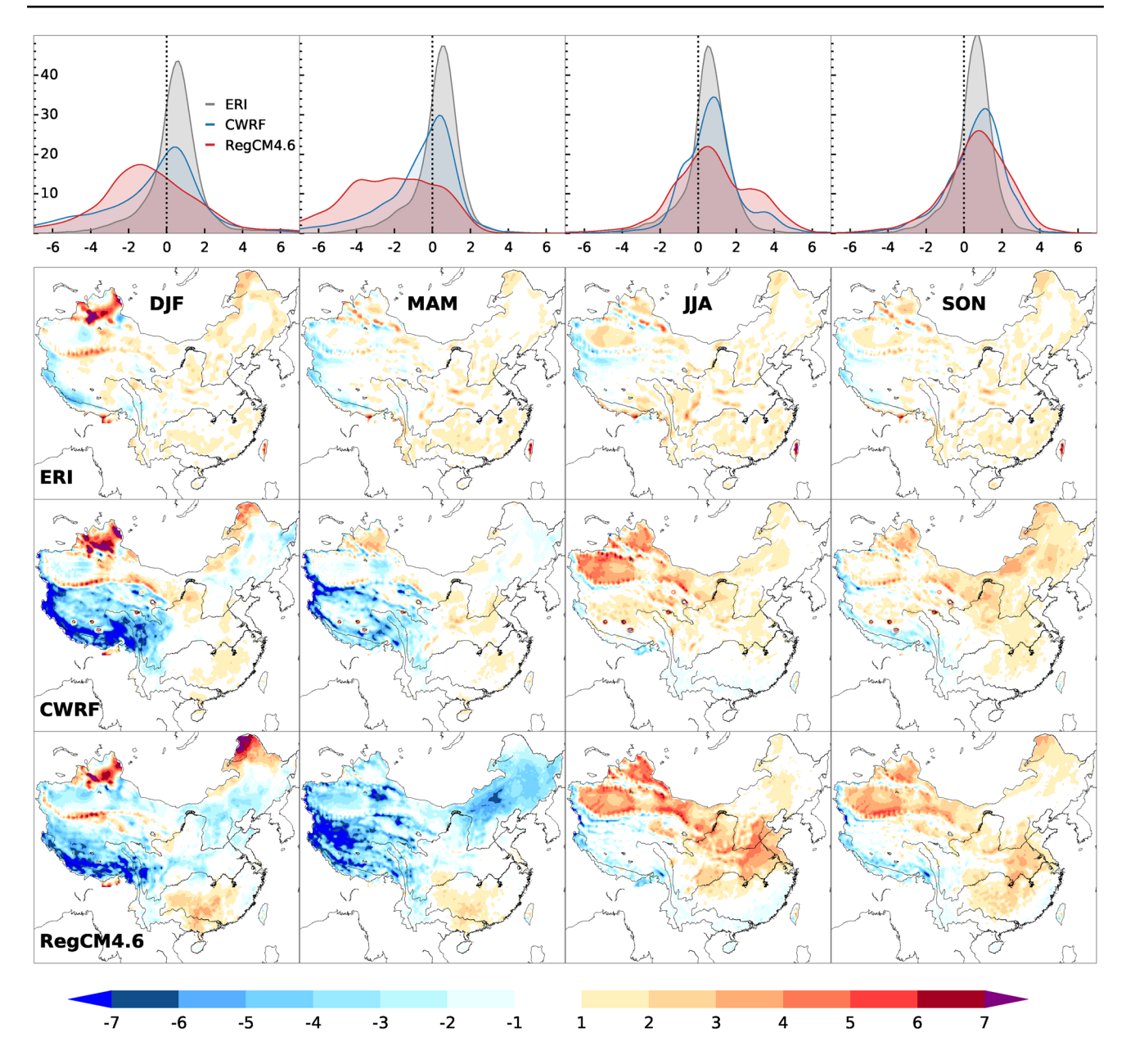


Fig. 5 Geographic distributions of ERI, CWRF and RegCM4.6 seasonal average biases (departures from observations) in daily mean temperature (°C) and their frequency distributions over Mainland

China. The biases colored on the maps are statistically significant at a confidence level better than 95% with a student test, assuming yearly independence

observations are abundant. One exception occurs between the Yellow and Yangtze Rivers, where CWRF overestimates the range by 1–3 °C in winter. This occurs as a combination of warmer maximum and colder minimum, suggesting insufficient cloud effects to reduce daytime incoming solar and nighttime outgoing infrared radiation. A similar but weaker CWRF bias pattern exists in spring. Additionally, CWRF underestimates the range in northern China areas of sparse observations, due mainly to warmer minimum temperatures. On the other hand, RegCM4.6 simulates significantly greater range biases, with overestimation to the south of the

Yangtze River and underestimation in western China and to the north of the Yellow River. This amplification is most severe in winter, strong in autumn, and notable in spring. Such patterns are mainly explained by biases in the daily maximum for winter and spring, but by the combination of warmer maximum south of the Yellow River and warmer minimum in northern China for autumn. These imply more complicated deficiencies in RegCM4.6. Future investigation should also consider the temperature range effect due to the precipitation diurnal cycle, which remains a modeling challenge (Liang et al. 2004a).



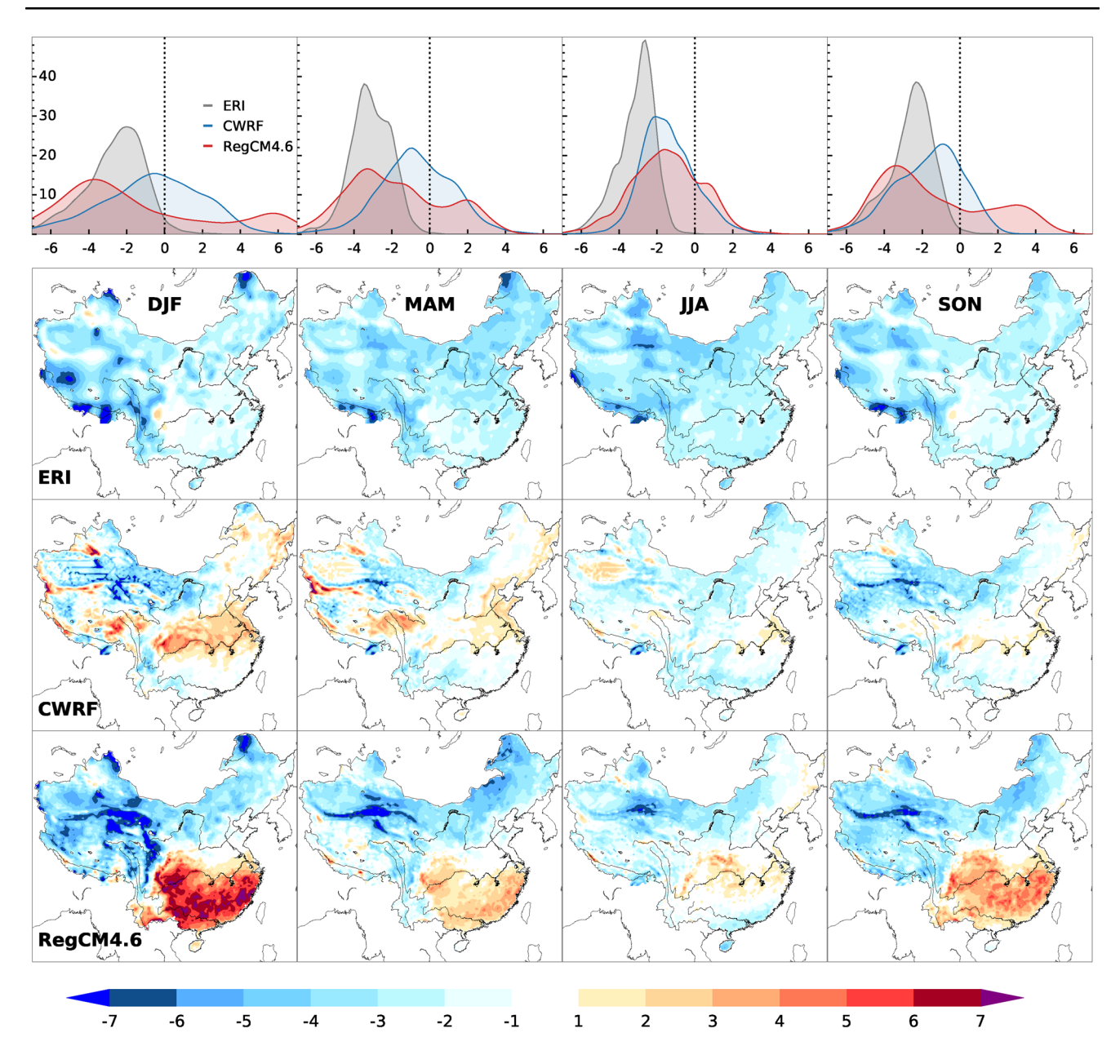


Fig. 6 Same as Fig. 5 except for daily temperature range (°C)

Some straight-line patterns appear in CWRF daily temperature range biases (Fig. 6) over the Taklamakan-Gobi Desert. Relative to the surrounding background, stronger negative range biases correspond to daily temperature colder maximum (Fig. S3) and warmer minimum (Fig. S4). They are identified with wetter soil moisture bands along with streamflow lines. Over the desert areas with relatively flat terrain, the existing digital elevation model data are inadequate to define actual streams and flow directions. The unrealistic specification of these and related SBCs causes CSSP to produce soil and air temperature departures from their references, which are also uncertain due to the lack of in situ observations. Correction to these deficiencies will

require realistic representation of the terrestrial hydrology, which depends on accurate SBCs and real verification data.

Figure 7 compares model performances for surface wind speed. The bias frequency indicates that CWRF is more realistic than ERI, with the peak near 0 rather than 1 (m s⁻¹) in all seasons. RegCM4.6 is worse than ERI, with the peak shifted to ~ 2 (m s⁻¹), indicating systematic overestimation. CWRF's superior performance is obvious in eastern China, where the model differs little from the reference that has abundant observations. In contrast, ERI contains overestimations of 1–2 (m s⁻¹) over broad regions like South China, persistent throughout the year. In western China, CWRF and ERI share a similar pattern in all seasons, with



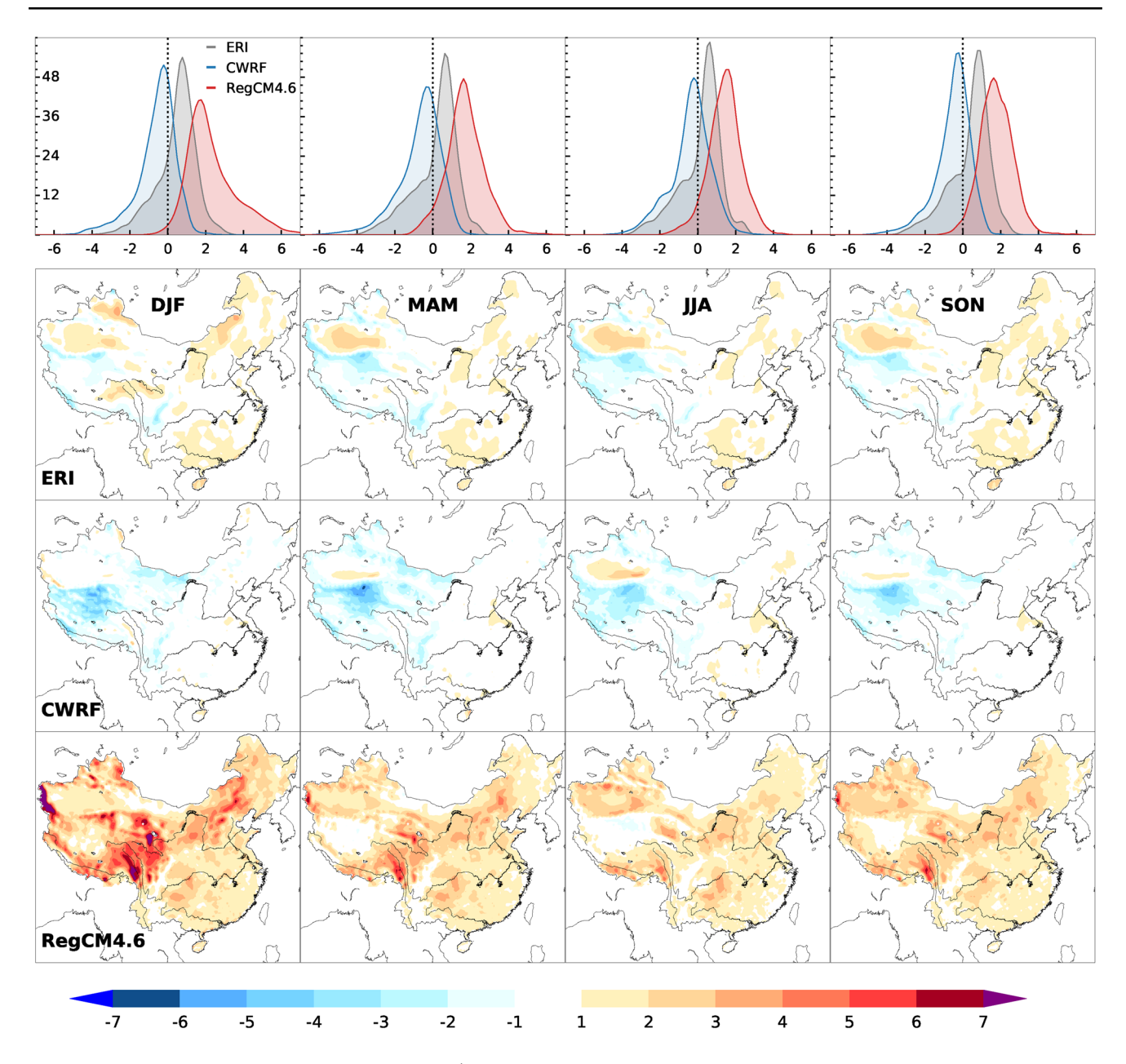


Fig. 7 Same as Fig. 6 except for surface wind speed (m s⁻¹)

underestimation in northern West Tibet and overestimation in South Xinjiang. However, RegCM4.6 overestimates most severely in East and South Tibet. Since there are very few observations in these regions, it is uncertain whether these biases reflect errors in the models or the reference data.

5 Interannual variation

Figure 8 compares CWRF- and RegCM4.6-simulated surface air temperature interannual temporal correlations with observations, including seasonal geographic maps

and frequency distributions over only eastern China (due to its abundant monitoring data). The correlations for ERI are all high (attributed to its effective surface data assimilation) and are not shown here. The CWRF correlations are very high from autumn to spring almost everywhere (except for South Xinjiang and West Tibet, where observations are lacking), indicating extraordinary model skill in capturing interannual temperature variations. Good performance is also seen in summer, except that most of Central to South China lacks useful skill. RegCM4.6 shares these performance features, although somewhat less skillful than



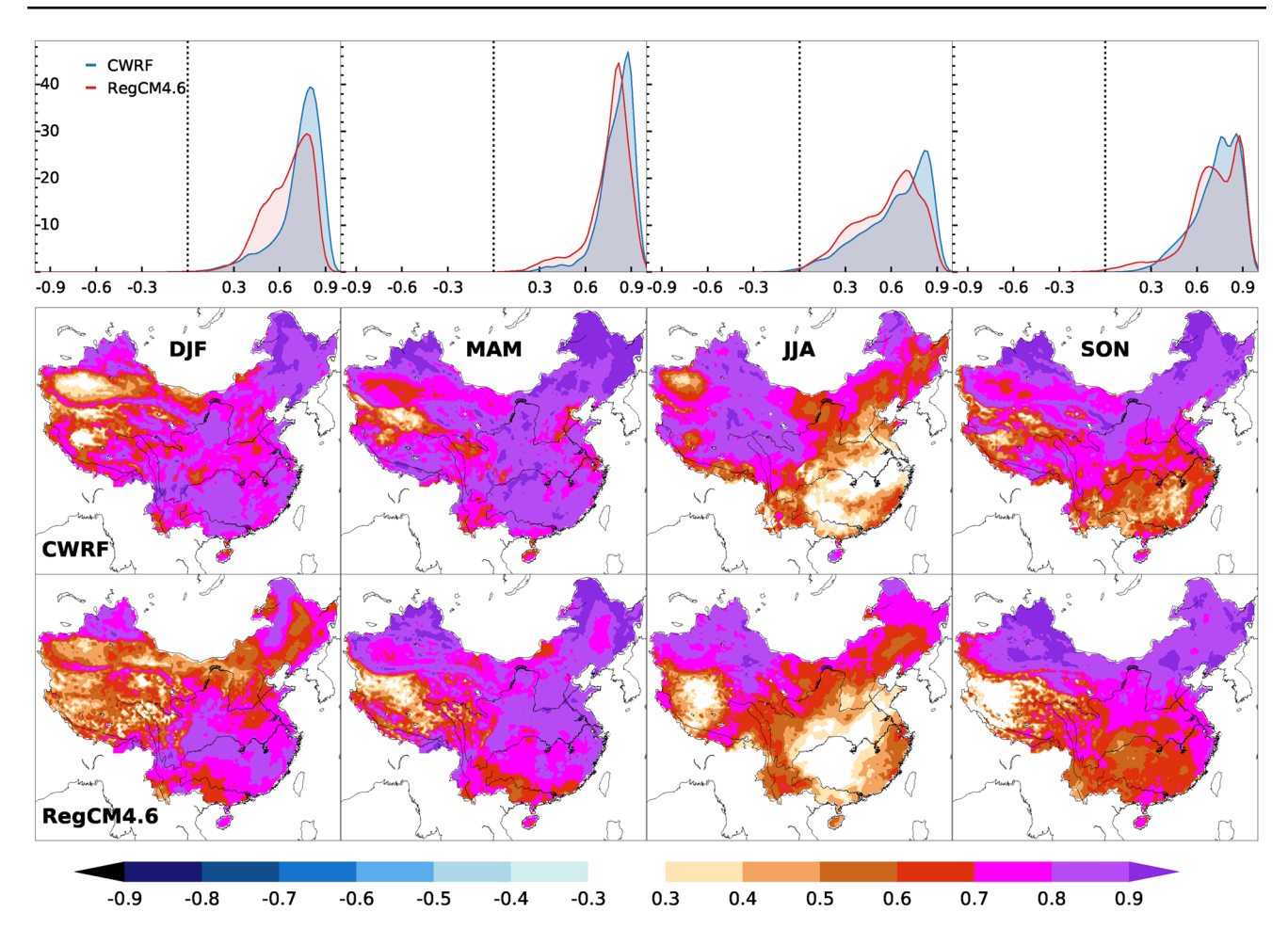


Fig. 8 Geographic distributions of CWRF and RegCM4.6 simulated temperature interannual correlations with observations and their frequency distributions over eastern China. The correlations larger than

0.3 as colored are statistically significant at a confidence level better than 95% with a student test, assuming yearly independence

CWRF, with the frequency peak or tail shifted to a smaller correlation, especially in winter and spring.

Figure 9 compares the precipitation correlations. CWRF performs very well in winter, with large, significant correlations almost everywhere in eastern China. Good performance is also seen in spring, except that correlations in the western part (105-110°E) of Central to South China and some portions of North and Northeast China are no longer significant. The area of significant correlations is further reduced in autumn, especially in North China and along the east coast. Overall performance is weakest in summer, when most areas along the Yangtze River to the south of the Yellow River lack significant correlations. For all seasons, RegCM4.6 has less overall skill in smaller areas than CWRF. Summer temperature in Central to South China consistently performs poorly in both CWRF and RegCM4.6 (Fig. 8). This consistency may indicate a challenging issue related to regional climate predictability during the summer monsoon, in which strong convective activities and land-seaair interactions occur. Large-scale circulation forcings via LBCs are no longer dominant, whereas regional factors and feedbacks become more critical. Thus, skill enhancement in this region will likely depend on incorporating surface data assimilation to improve initialization and system memory in terrestrial hydrology and coastal oceans (Kumar et al. 2008), and developing an optimized multi-physics ensemble to improve model representation of key processes such as convection-microphysics-radiation and surface-atmosphere interactions (Liang et al. 2012).

The covariability of precipitation and temperature is a key measure of a model's ability to capture coupled physical processes (Trenberth and Shea 2005). Figure 10 compares CWRF and RegCM4.6 simulations to observed precipitation-temperature interannual correlations for each season. Observations show strong negative correlations in summer over most of Central-South China, as well as in the northern and western parts of the Northeast, Inner Mongolia, the northern (western) parts of North (South) Xinjiang, and South Tibet. These latter regions have sparse data, so the reference itself is uncertain. The negative



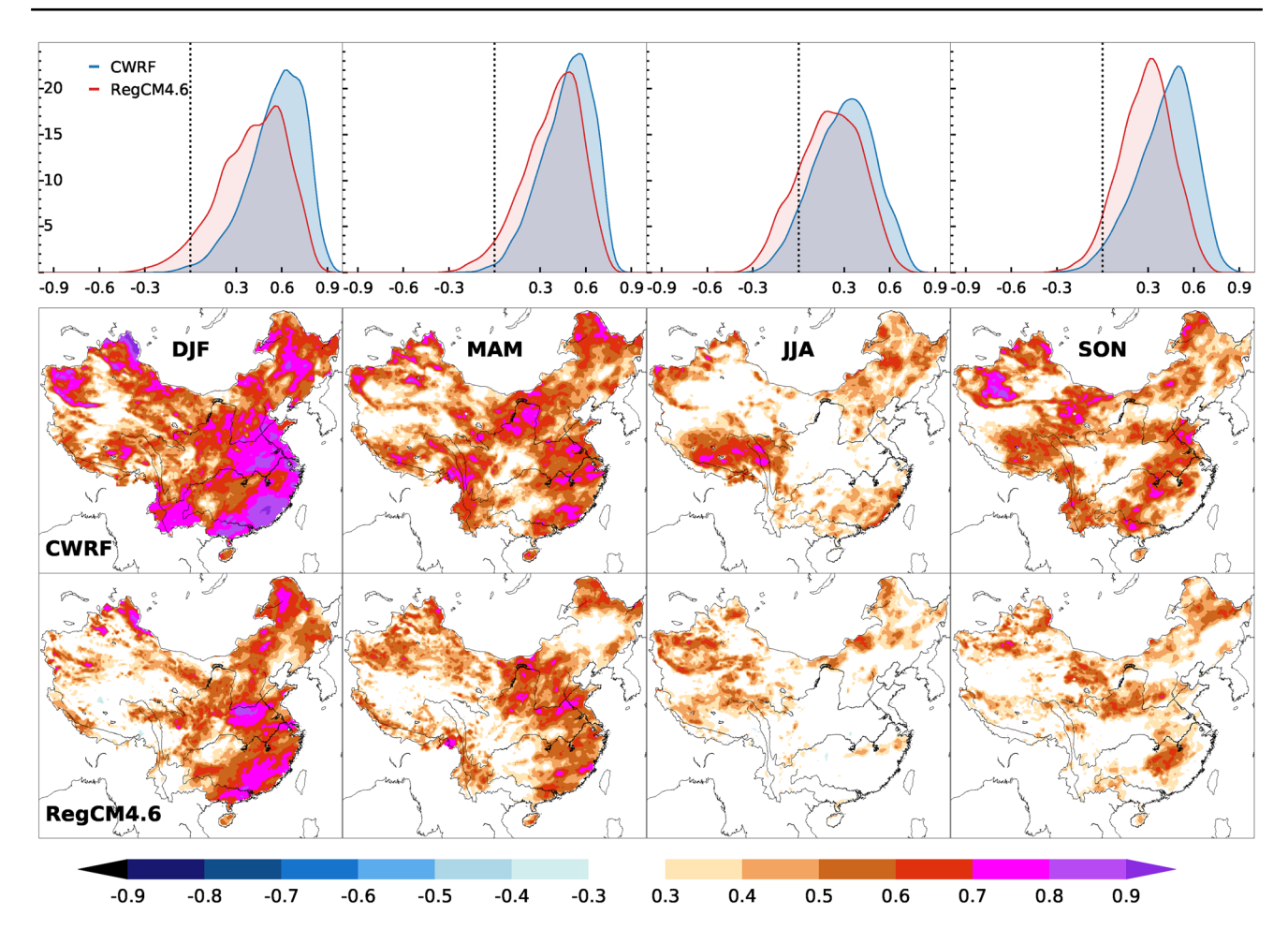


Fig. 9 Same as Fig. 8 except for precipitation

correlations reflect more solar heating and less evaporative cooling under dry conditions (Trenberth and Shea 2005). CWRF captures observations in eastern China well, with a little underestimation in South China. On the other hand, RegCM4.6 overestimates the relationship, especially in North China, indicating a too strong coupling between precipitation and temperature.

Other seasons show much weaker relationships. In spring, both models well simulate the strong observed negative correlations in the Southwest; CWRF overestimates and RegCM4.6 underestimates the weaker correlations between the Yangtze and Yellow Rivers; CWRF also overestimates correlations in the southeastern part of the Northeast. In autumn, observations exhibit weaker correlations, which RegCM4.6 underestimates in the Southwest but overestimates between the two rivers; in both counts CWRF is more realistic. In winter, CWRF well captures the strong negative correlations in the central Northeast, which RegCM4.6 underestimates; stronger correlations occur in the Southwest and extend to Sichuan, which CWRF simulates realistically but RegCM4.6 overestimates and expands further into the

area between the upper reaches of the Yangtze and Pearl Rivers.

In regions where RegCM4.6 simulates stronger precipitation negative correlations with temperature, it also overestimates positive correlations with relative humidity for all seasons (Fig. S5). Thus, RegCM4.6 overestimates the coupling between precipitation, temperature and humidity, indicating unrealistic cloud radiative and surface evaporative effects, especially in summer and autumn. This overestimation is likely because increased precipitation is associated with more clouds (so less solar heating) and wetter surfaces (so more evaporation), both of which favor warmer and moister near-surface air.

Interestingly, scattered regions of positive precipitation-temperature correlations appear in winter along the Yangtze River and Jiangsu's coast, as well as in spring in Inner Mongolia. Unlike RegCM4.6, CWRF captures both of these. Such positive correlations may result from precipitation favored by warm moist advection in extratropical cyclones and limited by low water availability in cold conditions (Trenberth and Shea 2005). In addition, CWRF



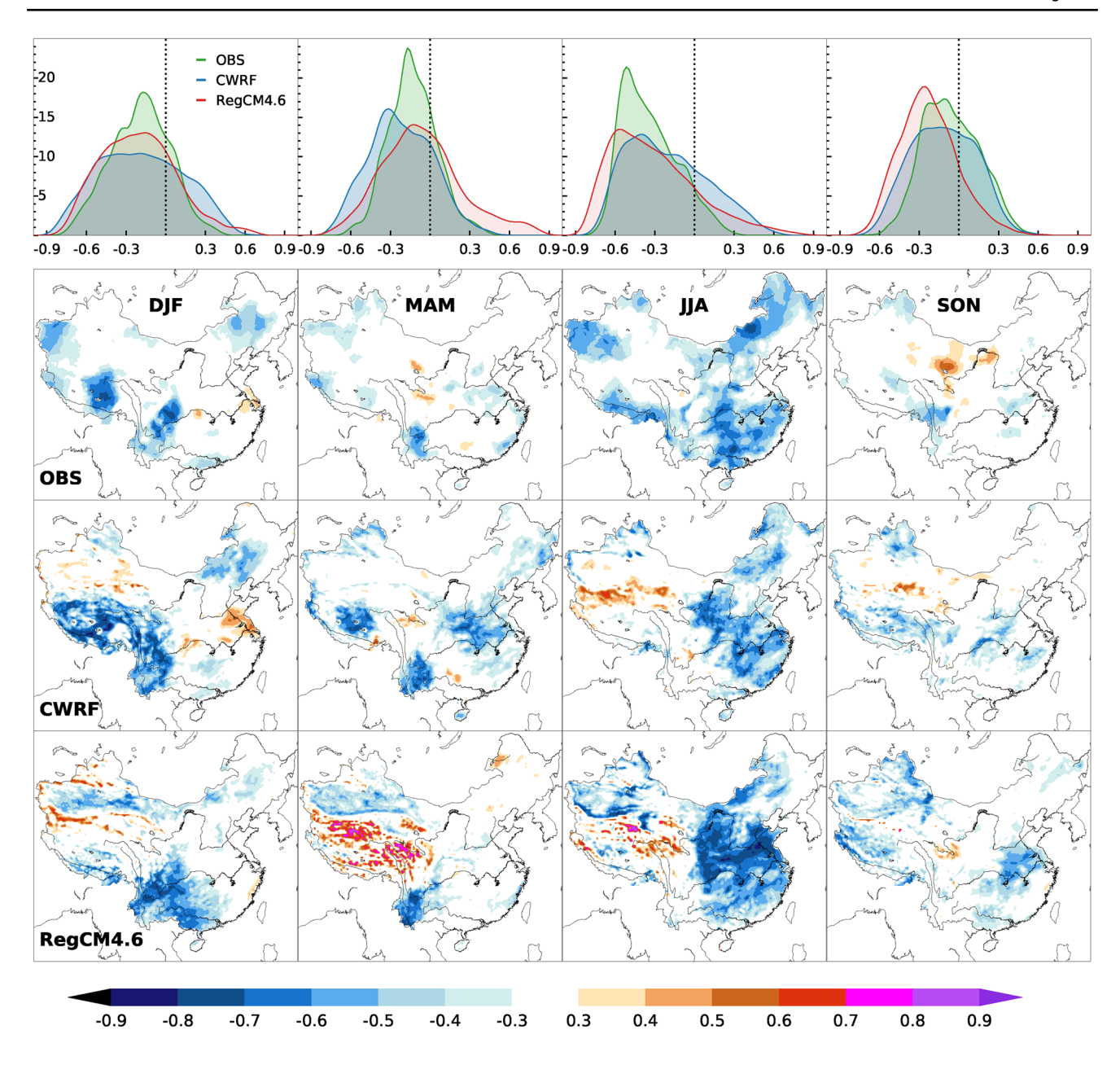


Fig. 10 Same as Fig. 8 except for cross correlations between precipitation and temperature observed (OBS) and simulated by CWRF and RegCM4.6

generates positive correlations along the northern slopes of the Tibetan Plateau, strong in summer and weaker in autumn and winter. Perhaps orographic uplift causes warm air holding large amounts of water to precipitate more, especially over these high elevation regions. In contrast, RegCM4.6 simulates positive correlations over the Tibetan Plateau, strong in spring and weaker in summer. Perhaps this precipitation is associated with low clouds that radiate back to warm the surface. However, such a regional relationship is either not evident or can even be reversed (such as in spring in West Tibet) in CWRF. Negative correlations over the Plateau are also simulated by CWRF in winter (strong) and by

both models in autumn (weaker). Observational data over the Plateau are needed to understand the actual processes responsible for these positive correlations.

Figures 11 and 12 compare CWRF and RegCM4.6 simulations with observed temperature and precipitation monthly anomalies during 1980–2015, averaged over the five regions with relatively dense monitoring stations (Southwest, South China, Central China, North China, Northeast). They are normalized against their own mean annual cycles of the same period, with the respective monthly means and interannual standard deviations also shown. As in the earlier discussion, the mean temperature



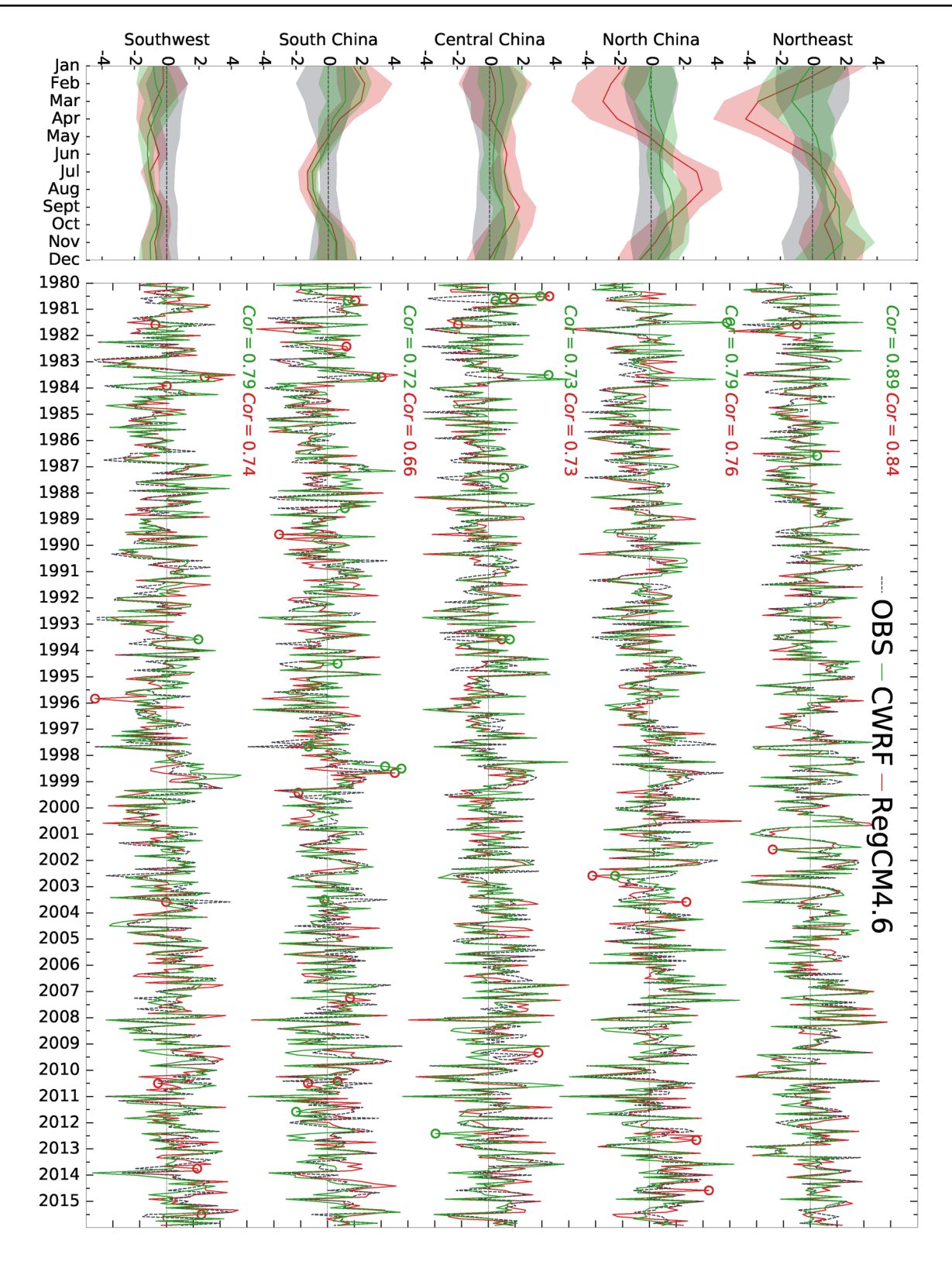


Fig. 11 The 1980–2015 mean and standard deviation annual cycles (left, C) and normalized interannual anomalies (right) of temperature simulated by CWRF and RegCM4.6 along with observations (OBS)

as averaged over the five key regions with good data. The models mean annual cycle is shown as monthly departures from observations



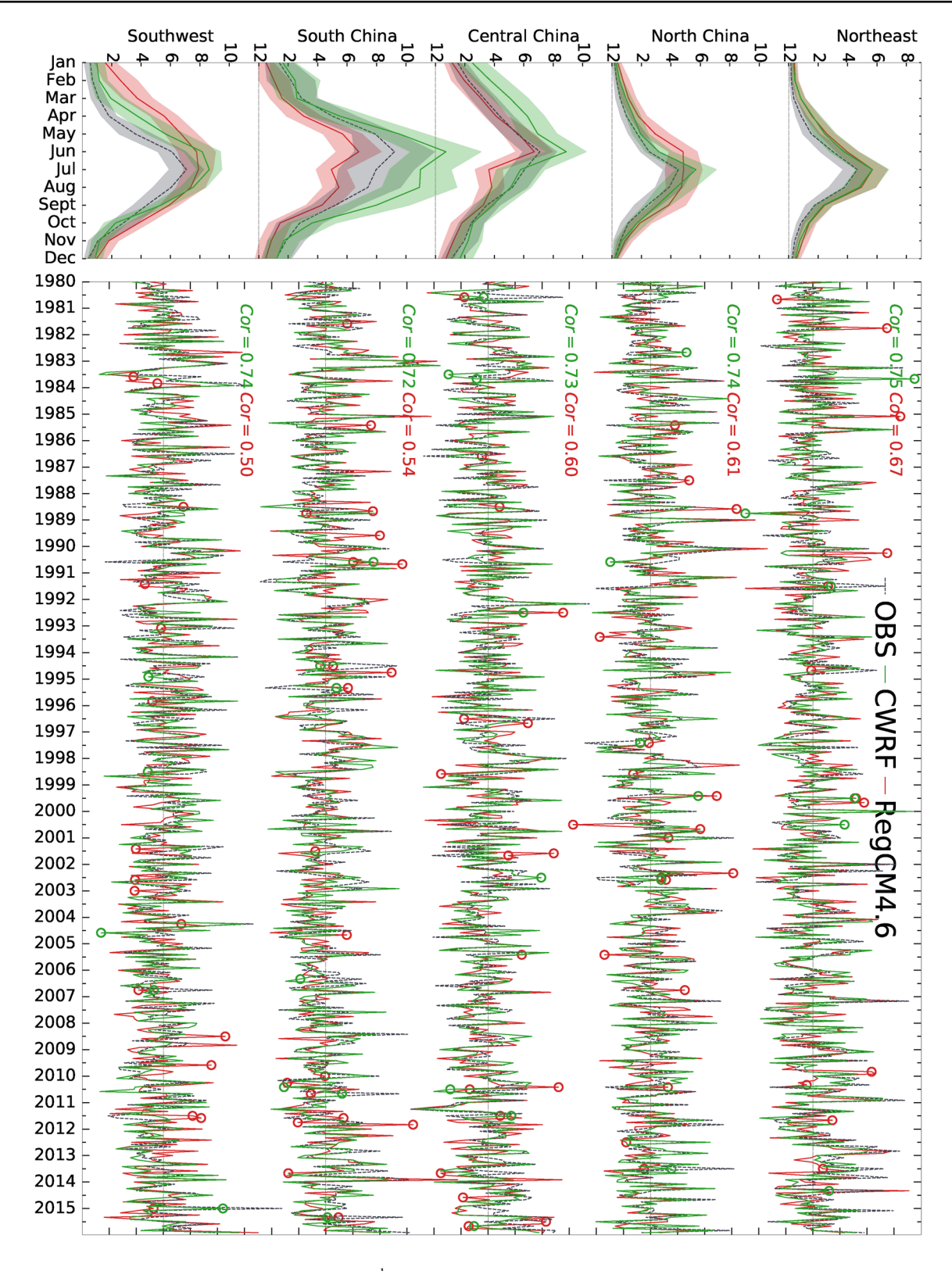


Fig. 12 Same as Fig. 11 except for precipitation (mm day⁻¹)



annual cycle is depicted as the departure from observations. The results for the six regions with sparse data records (Inner Mongolia, East Tibet, South Tibet, West Tibet, South Xinjiang, North Xinjiang) are illustrated in Figs. S6, S7.

For the five regions with good data, CWRF simulates the annual cycle for both temperature and precipitation more realistically overall than RegCM4.6. In particular, RegCM4.6 is too cold from February to April in the Northeast and North China, and also too hot from July to September in North China. On the other hand, in Central China CWRF overestimates precipitation from January to June, while RegCM4.6 underestimates it from July to December; otherwise, both are realistic. In South China, RegCM4.6 underestimates precipitation throughout the year, while CWRF overestimates it from May to September. In both regions, the combination of the two models can better simulate observations, suggesting the advantage of an ensemble approach. Similarly, CWRF performs better than RegCM4.6 in the six regions with sparse data.

Temperature interannual anomaly correlations with observations are higher for CWRF than RegCM4.6 in all regions except North China (equal) and South Xinjiang (smaller). Correlation differences between the models are generally within 0-0.06, but are substantially larger in South Tibet (0.12), East Tibet (0.11), West Tibet (0.21), and South Xinjiang (-0.14), all areas with sparse data and thus less confidence. Likewise, precipitation interannual anomaly correlations with observations are higher for CWRF than RegCM4.6 in all regions, with notably larger differences in the Southwest (0.24), South China (0.19), Central China (0.13), North China (0.15), and the Northeast (0.08), all of which have good data, as well as in Inner Mongolia (0.08), East Tibet (0.15), West Tibet (0.11), and North Xinjiang (0.16), which have sparse data. These results indicate that CWRF better captures observed characteristics of interannual anomalies along with a more realistic annual cycle than RegCM4.6, especially for precipitation over most regions in China.

It is important to identify the key regional anomalies that substantially differ between models and observations. A subsequent diagnostic analysis of these anomalies will offer insight into the climate processes and physical mechanisms that cause such model deficiencies. We choose 2.0 as the threshold that the absolute difference in normalized anomalies between simulated and observed must exceed. These exceedances contain substantial model errors that require future investigation to improve seasonal prediction skill. As marked in Figs. 11, 12 and S6, S7, these cases occur less frequently in CWRF than RegCM4.6, especially for precipitation. The overall results, including exceptions, are consistent with those revealed above in correlations. However, these cases are not coherent between precipitation and

temperature, nor between the models and among the regions, indicating that process diagnosis will be challenging.

6 Extreme precipitation

CWRF and RegCM4.6 performance relative to ERI in simulating the 1980-2015 mean 95th percentile of daily precipitation in each season over Mainland China is summarized in a Taylor diagram (Fig. 13). CWRF exhibits outstanding performance in all seasons, producing a high pattern correlation (0.79–0.90) and realistic spatial variability (0.96–1.09), improving over ERI's smaller correlation (0.71–0.88, except for autumn) and systematic lower variability (0.70–0.87). RegCM4.6 produces reasonable variability (0.85–1.01) but a significantly lower correlation (0.59-0.78) than CWRF and ERI throughout the year. For the larger 99th percentile (not shown), CWRF performance remains high with an even better correlation (0.84-0.91) but slightly larger variability (1.05-1.16). On the other hand, the RegCM4.6 performance is further degraded, with an even lower correlation (0.48–0.69) and a systematically reduced variability (0.78-0.86).

Figure 14 compares seasonal geographic distributions of the 1980–2015 mean 95th percentile of daily precipitation. In summer, large rainfall (>30 mm day⁻¹) occurs over wide areas extending from South, Central and North China to the southern coast of the Northeast Plain. A band of maxima (exceeding 40 mm day⁻¹) exists along both the Yangtze and Pearl Rivers. ERI systematically underestimates

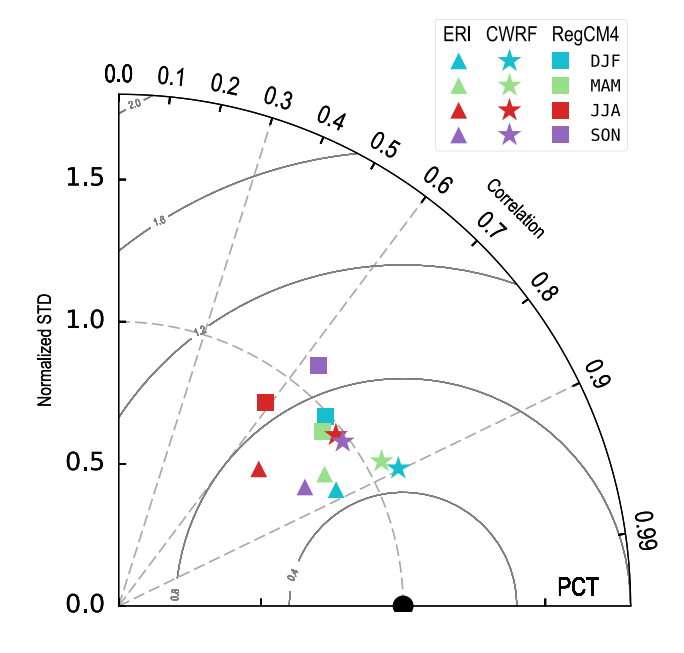


Fig. 13 Same as Fig. 2 except for the 95th percentile of daily precipitation



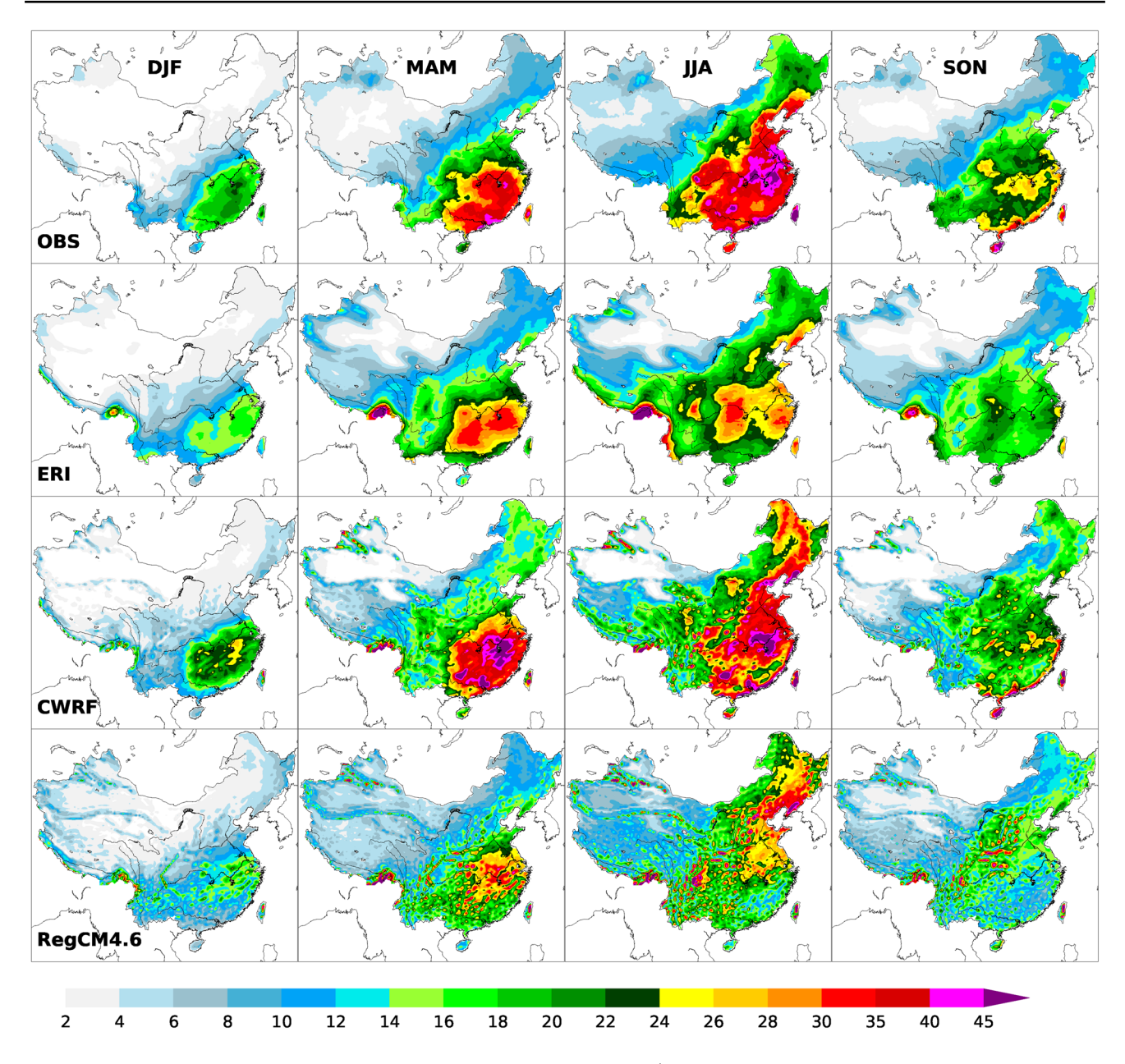


Fig. 14 Same as Fig. 3 except for the 95th percentile of daily precipitation (mm day⁻¹)

the extremes, especially in Southeast China, roughly capturing only the centers along the Yangtze River, though even these are displaced. Similarly, RegCM4.6 fails to simulate the Pearl River band and also underestimates the Yangtze River band. In contrast, CWRF realistically reproduces the location and magnitude of the centers along both rivers. The extremes along the Northeast Plain coast are well captured by both CWRF and RegCM4.6, but largely underestimated by ERI. CWRF generates another band of large precipitation along the three mountain ridges surrounding the Northeast Plain. These peaks are very weak in ERI and RegCM4.6, as well as in the reference data. As discussed

earlier, monitoring stations along these ridges are rare, and thus the ground truth is not known.

The comparative summer features above are generally retained in spring. The area of large rainfall (> 30 mm day⁻¹) shrinks, losing North China and the Northeast Plain coast, but the two bands of maxima remain along the Yangtze and Pearl Rivers. CWRF realistically captures this characteristic better than ERI and RegCM4.6, which both miss the Pearl River band. The increased correlation in the Taylor diagram shows that the spring patterns produced by ERI, CWRF, and RegCM4.6 are all more realistic than the respective summer patterns. This improvement tendency is also seen from



spring to winter, when the percentile magnitude is reduced below 25 mm day⁻¹. As a transition toward the dry winter monsoon, the autumn pattern resembles that of summer but with a systematic reduction in magnitude. Observations still show a band of maxima close to 25 mm day⁻¹ along the Yangtze River. This is visible in CWRF but more scattered, whereas it is further weaker in ERI and displaced to the west in RegCM4.6. Another key feature in autumn is the large rainfall band along China's entire southeastern coast. This feature is well captured by CWRF and RegCM4.6, but totally missed in ERI. These results indicate that the RCMs are better able to resolve rainfall enhancement by sea breezes along the coast than the coarser ERI.

7 Conclusion

The performance of CWRF for modeling regional climate in China has been rigorously evaluated relative to the most popular RegCM4.6 and the driving ERI through intercomparison of historical simulations during 1980-2015. The comparison focuses on the ability to reproduce the annual cycle, interannual variation, and extreme statistics including precipitation and surface temperature. It is demonstrated that CWRF performs better overall than RegCM4.6, as measured by various quantitative metrics such as bias, correlation, intensity, frequency, and extremes. In particular, CWRF captures the two major summer monsoon rain bands along the Yangtze River and across South China more realistically than RegCM4.6 and even ERI, despite the latter's assimilation of surface observations. CWRF better represents the diurnal temperature range throughout the year, which ERI systematically underestimates, while RegCM4.6 enhances both negative and positive biases. It improves representation of surface wind, which ERI and especially RegCM4.6 overestimate. For all seasons, CWRF has more skill than RegCM4.6 in simulating interannual anomalies of precipitation and temperature as well as their couplings with humidity. Furthermore, CWRF exhibits outstanding performance in reproducing the 95th percentile of daily precipitation, which ERI persistently underestimates and RegCM4.6 simulates with less coherence. In all ranges of intensity for both daily and monthly precipitation, CWRF generates consistently higher scores than RegCM4.6.

It is challenging to identify which formulation differences listed in Table 2 explain the better performance of CWRF over RegCM4.6. Unexpectedly, increasing the vertical resolution to match CWRF further degrades the RegCM4.6 performance in all the metrics presented above, especially for precipitation related quantities. On the other hand, experiments varying CWRF physics configurations among alternative cumulus, microphysics, cloud, aerosol, radiation, PBL, and surface schemes reveal different levels of sensitivity. In

summer, the primary sensitivity comes from the cumulus parameterization, where the CWRF default ECP scheme (Qiao and Liang 2016a, b) simulates more realistic monsoon precipitation characteristics than that used in RegCM4.6 (Tiedtke 1989). The secondary sensitivity lies in cloud-radiation and PBL-surface interactions, while microphysics and aerosol effects are relatively minor. However, the sensitivities change between seasons and variables. A comprehensive study of these sensitivities, which is underway, may help understand key physics parameterizations attributable to the CWRF-RegCM4.6 performance difference. Nonetheless, the comparative results presented in this study justify the initial release of the latest CWRF model together with its computational domain, comprehensive SBCs, and physics configuration, all of which are well tested at 30 km grid spacing for regional climate modeling applications over China.

This CWRF release has no intention to discourage the continuous use of RegCM4.6 or any other RCMs. In fact, the RegCM4.6 performance presented above is based on a single realization with a typical physics configuration conveniently available to us. RegCM4.6 currently includes 3 surface, 2 PBL, 2 microphysics, 6 cumulus, and 2 radiation schemes, so that 144 combinations can be configured. A systematic assessment of the RegCM4.6 performance with various physics configurations is yet to be conducted and compared more appropriately at the same finer vertical resolution as in CWRF. Similarly, CWRF has incorporated many more alternate physics schemes than are presented here, with the total combinations exceeding available computing resources to fully examine (Liang et al. 2012; Liang and Zhang 2013), and the skill of each configuration possibly depending on both horizontal and vertical resolutions. The released version likely does not represent the best performance of CWRF, since only a tiny set of its physics configurations has been tested. A more desirable approach would be an ensemble of multiple physics configurations of CWRF or RegCM4.6 or multiple RCMs. Such an ensemble approach can incorporate performance-based weighting for individual member's contributions to optimize the outcome, offering a pragmatic way to enhance regional climate prediction skill (Liang et al. 2012). Furthermore, observational data at a finer resolution comparable to the model grid are needed. The available data used in this study are inadequate, especially in western China, causing large uncertainties in model performance evaluation. These are areas of future research focus, some of which are in progress.

Acknowledgements The RCM simulations were made using the Maryland Advanced Research Computing Center's Bluecrab and the University of Maryland Deepthought HPC clusters for CWRF, and the Institute of Atmospheric Physics/Chinese Academy of Sciences supercomputing resources for RegCM4.6. The gridded analysis surface data as the observational reference were provided by China Meteorological Administration (CMA). Liang was partially supported by U.S.



National Science Foundation Innovations at the Nexus of Food, Energy and Water Systems under Grant EAR-1639327 and CMA/National Climate Center research subcontract (2212031635601), Zheng by the Chinese Scholar Council fellowship, Dai by the National Key Research and Development Program of China (2017YFA0604303), Choi by the National Research Foundation of Korea (2017R1A2B4005232), Ling by the National Natural Science Foundation of China (NSFC) (41376016), Qiao by China Postdoctoral Science Foundation (2014M561437), Bin by NSFC (41575089), and Wang by NSFC (41275077). We thank Jennifer Kennedy for thorough editing and Qing Sun for GIS mapping.

TDK Tiedtke convective scheme

UOM Upper ocean model

United states geological survey UW University of Washington moist turbulence

parameterization

WRF Weather research and forecasting model **XRL** Xu-Randall-Liang cloud

parameterization

Appendix A: Acronyms and Abbreviations

CAR Cloud aerosol radiation

CCLM COSMO (Consortium for Small Scale Model-

ling) Climate local model

CLM Community land model Community climate model **CCM**

CSSP Conjunctive surface-subsurface process model

CAM Community atmosphere model **CMA** China Meteorological Administration

CSSP Conjunctive surface-subsurface process model

CWRF Climate-weather research and forecasting

model

ECP Ensemble cumulus parameterization

ECMWF European Centre for Medium-Range Weather

Forecasts

ERI ECMWF reanalysis interim

GRIMs Global/regional integrated model system GSFCLXZ Goddard Space Flight Center Liang, Xin-

zhong radiation scheme

GSFCGCE Goddard Space Flight Center Goddard Cumu-

lus Ensemble

IGBP International geosphere-biosphere programme

IPRC International Pacific Research Center model

JSM Japan spectral model

LMDZ Laboratoire de météorologie dynamique-zoom

model

LISSS Lake ice snow and sediment simulator **MISR** Multiangle imaging spectra radiometer MM5 Fifth-generation mesoscale model

MODIS Moderate resolution imaging

spectroradiometer

PRECIS Providing regional climates for impacts studies

RAMS Regional atmospheric modeling system RegCM Regional climate modeling system

RIEMS Regional integrated environment model

system

RMIP Regional model intercomparison project

RSM Regional spectral model

SUBEX Subgrid explicit moisture scheme

References

USGS

Banzon V, Smith TM, Chin TM, Liu C, Hankins W (2016) A long-term record of blended satellite and in situ sea-surface temperature for climate monitoring, modeling and environmental studies. Earth Syst Sci Data 8:165-176

Bao J, Feng J, Wang Y (2015) Dynamical downscaling simulation and future projection of precipitation over China. J Geophys Res 120:8227-8243. https://doi.org/10.1002/2015JD023275

Bonan GB, Levis S, Kergoat L, Oleson KW (2002) Landscapes as patches of plant functional types: an integrating concept for climate and ecosystem models. Global Biogeochem Cycles 16:5. https://doi.org/10.1029/2000GB001360

Bretherton CS, Park S (2009) A new moist turbulence parameterization in the Community Atmosphere Model. J Climate 22:3422–3448

Bucchignani E, Montesarchio M, Cattaneo L, Manzi MP, Mercogliano P (2014) Regional climate modeling over China with COSMO-CLM: Performance assessment and climate projections. J Geophys Res 119(12):151-112170

Cha D-H, Jin CS, Moon JH, Lee DK (2016) Improvement of regional climate simulation of East Asian summer monsoon by coupled air-sea interaction and large-scale nudging. Int J Climatol 36:334-345

Chan JC, Liu Y, Chow KC, DING Y, Lau WK, Chan KL (2004) Design of a regional climate model for the simulation of South China summer monsoon rainfall. J Meteorol Soc Jpn Ser II 82(6):1645-1665

Chen W, Jiang Z, Li L, Yiou P (2011) Simulation of regional climate change under the IPCC A2 scenario in southeast China. Clim Dyn 36:491-507

Chen L, Liang X-Z, DeWitt D, Samel AN, Wang JXL (2016) Seasonal prediction of US precipitation and temperature by the nested CWRF-ECHAM system. Clim Dyn 46:879–896

Choi HI, Liang X-Z (2010) Improved terrestrial hydrologic representation in mesoscale land surface models. J Hydrometeorol 11:797-809

Choi HI, Kumar P, Liang X-Z (2007) Three-dimensional volumeaveraged soil moisture transport model with a scalable parameterization of subgrid topographic variability. Water Resour Res 43:W04414. https://doi.org/10.1029/2006WR005134 15 pp.

Choi HI, Liang X-Z, Kumar P (2013) A conjunctive surface-subsurface flow representation for mesoscale land surface models. J Hydrometeorol 14:1421-1442

Chou M-D, Suarez MJ (1999) A solar radiation parameterization for atmospheric studies. [Last revision on March 2002] Technical Report Series on Global Modeling and Data Assimilation. M. J. Suarez (Ed.), NASA/TM-1999-104606, Vol. 15, Goddard Space Flight Center, Greenbelt, MD, 42 pp

Chou M-D, Suarez MJ, Liang X-Z, Yan MM-H (2001) A thermal infrared radiation parameterization for atmospheric studies. [Last revision on July 2002] Technical Report Series on Global Modeling and Data Assimilation, M.J. Suarez (Ed.), NASA/



- TM-2001-104606, Vol. 19, Goddard Space Flight Center, Greenbelt, MD, 56 pp
- Chow KC, Tong H-W, Chan JCL (2008) Water vapor sources associated with the early summer precipitation over China. Clim Dyn 30:497_517
- Christensen JH, Carter TR, Rummukainen M, Amanatidis G (2007) Evaluating the performance and utility of regional climate models: The PRUDENCE project. Clim Change 81:1–6
- Dai Y, Zeng X, Dickinson RE, Baker I, Bonan GB, Bosilovich MG, Denning AS, Dirmeyer PA, Houser PR, Niu G, Oleson KW, Schlosser CA, Yang Z-L (2003) The common land model. Bull Am Meteorol Soc 84:1013–1023
- Dai Y, Dickinson RE, Wang Y-P (2004) A two-big-leaf model for canopy temperature, photosynthesis, and stomatal conductance. J Climate 17:2281–2299
- Daly C, Neilson RP, Phillips DL (1994) A statistical-topographic model for mapping climatological precipitation over mountainous terrain. J Appl Meteorol 33:140–158
- Dee DP, Uppala SM, Simmons AJ, Berrisford P, Poli P, Kobayashi S, Andrae U, Balmaseda MA, Balsamo G, Bauer P, Bechtold P, Beljaars ACM, van de Berg L, Bidlot J, Bormann N, Delsol C, Dragani R, Fuentes M, Geer AJ, Haimberger L, Healy SB, Hersbach H, Hólm EV, Isaksen L, Kållberg P, Köhler M, Matricardi M, McNally AP, Monge-Sanz BM, Morcrette JJ, Park BK, Peubey C, de Rosnay P, Tavolato C, Thépaut JN, Vitart F (2011) The ERA-Interim reanalysis: configuration and performance of the data assimilation system. Quart J Meteorol Soc 137:553–597
- Fang YJ, Zhang YC, Huang AN, Li B (2013) Seasonal and intraseasonal variations of East Asian summer monsoon precipitation simulated by a regional air–sea coupled model. Adv Atmos Sci 30(2):315–329
- Feng JM, Fu CB (2006) Inter-comparison of 10-year precipitation simulated by several RCMs for Asia. Adv Atmos Sci 23:531–542
- Feng JM, Wang YL, Fu CB (2011) Simulation of extreme climate events over China with different regional climate models. Atmos Oceanic Sci Lett 4:47–56
- Fischer T, Menz C, Su B, Scholten T (2013) Simulated and projected climate extremes in the Zhujiang River Basin, South China, using the regional climate model COSMO-CLM. Int J Climatol 33:2988–3001
- Fu CB, Wang SY, Xiong Z, Gutowski WJ, Lee DK, McGregor JL, Sato Y, Kato H, Kim JW, Suh MS (2005) Regional climate model intercomparison project for Asia. Bull Am Meteorol Soc 86:257–266
- Gao X-J, Zhao ZC, Ding YH, Huang RH, Giorgi F (2001) Climate change due to greenhouse effects in China as simulated by a regional climate model. Adv Atmos Sci 18:1224–1230
- Gao X-J, Zhao ZC, Giorgi F (2002) Changes of extreme events in regional climate simulations over East Asia. Adv Atmos Sci 19:927–942
- Gao X-J, Luo Y, Lin WT, Zhao ZC, Giorgi F (2003) Simulation of effects of landuse change on climate in China by a regional climate model. Adv Atmos Sci 20:583–592
- Gao X-J, Xu Y, Zhao ZC, Pal JS, Giorgi F (2006) On the role of resolution and topography in the simulation of East Asia precipitation. Theor Appl Climatol 86:173–185
- Gao X-J, Shi Y, Song R, Giorgi F, Wang Y, Zhang D (2008) Reduction of future monsoon precipitation over China: comparison between a high resolution RCM simulation and the driving GCM. Meteorol Atmos Phys 100:73–86
- Gao X-J, Shi Y, Giorgi F (2011) A high resolution simulation of climate change over China. Sci China Earth Sci 54(3):462–472
- Gao X-J, Shi Y, Zhang D, Wu J, Giorgi F, Ji Z, Wang Y (2012) Uncertainties in monsoon precipitation projections over China: results from two high-resolution RCM simulations. Clim Res 52:213–226. https://doi.org/10.3354/cr01084

- Gao X-J, Wang M-L, Giorgi F (2013) Climate change over China in the 21st century as simulated by BCC_CSM1.1-RegCM4.0. Atmos Oceanic Sci Lett 6:381–386. https://doi.org/10.3878/j. issn.1674-2834.13.0029
- Gao Y, Xu J, Chen D (2015) Evaluation of WRF mesoscale climate simulations over the Tibetan Plateau during 1979–2011. J Climate 28:2823–2841
- Gao X-J, Shi Y, Giorgi F (2016) Comparison of convective parameterizations in RegCM4 experiments over China with CLM as the land surface model. Atmos Ocean Sci Lett. https://doi.org/10.1080/16742834.2016.1172938
- Giorgi F (2006) Regional climate modeling: status and perspectives. J Phys IV France 139:101–118
- Giorgi F, Gutowski WJ (2015) Regional dynamical downscaling and the CORDEX initiative. Annu Rev Environ Resour 40:467–490
- Giorgi F, Marinucci MR, Bates G (1993a) Development of a second generation regional climate model (RegCM2). I. Boundary layer and radiative transfer processes. Mon Weather Rev 121:2794–2813
- Giorgi F, Marinucci MR, Bates G, DeCanio G (1993b) Development of a second generation regional climate model (RegCM2). II. Convective processes and assimilation of lateral boundary conditions. Mon Weather Rev 121:2814–2832
- Giorgi F, Coppola E, Solmon F, Mariotti L, Sylla MB, Bi X, Elguindi N, Diro GT, Nair V, Giuliani G, Turuncoglu UU, Cozzini S, Güttler I, O'Brien TA, Tawfik AB, Shalaby A, Zakey AS, Steiner AL, Stordal F, LC Brankovic (2012) RegCM4: model description and preliminary tests over multiple CORDEX domains. Climate Res 52:7–29
- Grell GA, Dudhia J, Stauffer DR (1994) A description of the fifthgeneration Penn State/NCAR Mesoscale Model (MM5). NCAR Tech, Boulder (Note NCAR/TN-398 + STR), 121 pp
- Gu HH, Wang GL, Yu ZB, Mei R, Tang JP, Wang SY (2012) Assessment on impact of climate change on East and South Asia using the RegCM4 regional climate model. Clim Change 114(7):301–317
- Guo J, Huang G, Wang X, Lin Q (2017) Investigating future precipitation changes over China through a high-resolution regional climate model ensemble. Earth's Future. https://doi.org/10.1002/2016EF000433
- Han W, Zhai P, 2015: Three cluster methods in regionalization of temperature zones in China. Clim Environ Res, 20(1):111–118 (in Chinese)
- Holtslag AAM, Boville BA (1993) Local versus nonlocal boundary-layer diffusion in a global climate model. J Clim 6:1825–1842
- Holtslag AAM, De Bruijn EIF, Pan HL (1990) A high resolution air mass transformation model for short-range weather forecasting. Mon Weather Rev 118:1561–1575
- Hu BY, Tang JP, Wang SY (2013) Evaluation and projection of extreme events over China under IPCC A1B scenario by MM5v3 model. Chin J Geophys 56(7):2195–2206 (in Chinese)
- Huang W-R, Chan JCL, Au-Yeung AYM (2013) Regional climate simulations of summer diurnal rainfall variations over East Asia and Southeast China. Clim Dyn 40:1625–1642. https://doi. org/10.1007/s00382-012-1457-2
- Huang D, Zhu J, Zhang Y, Huang Y, Kuang X (2016) Assessment of summer monsoon precipitation derived from five reanalysis datasets over East Asia. QJR Meteorol Soc 142:108–119. https://doi.org/10.1002/qj.2634
- Hui P, Tang J, Wang S, Wu J, Kang Y, 2014: Future climate projection under IPCC A1B scenario in the source region of Yellow River with complex topography using RegCM3. J Geophys Res Atmos, 119(11)205–11222, https://doi.org/10.1002/2014JD021992
- Hwang J-N, Lay S-R, Lippman A (1994) Nonparametric multivariate density estimation: a comparative study. IEEE Trans Signal Process 42(10):2795–2810



- Ji Z, Kang S (2015) Evaluation of extreme climate events using a regional climate model for China. Int J Climtol 35:888–902
- Kahn RA, Gaitley BJ, Martonchik JV, Diner DJ, Crean KA, Holben B, 2005: Multiangle Imaging Spectroradiometer (MISR) global aerosol optical depth validation based on 2 years of coincident Aerosol Robotic Network (AERONET) observations. J Geophys Res, 110, D10S04. https://doi.org/10.1029/2004JD004706
- Kahn RA, Garay MJ, Nelson DL, Yau KK, Bull MA, Gaitley BJ, Martonchik JV, Levy RC (2007) Satellite-derived aerosol optical depth over dark water from MISR and MODIS: Comparisons with AERONET and implications for climatological studies. J Geophys Res 112:D18205. https://doi.org/10.1029/2006JD008175
- Kang H-S, Hong S-Y (2008) Sensitivity of the simulated East Asian summer monsoon climatology to four convective parameterization schemes. J Geophys Res 113:D15119. https://doi. org/10.1029/2007JD009692
- Kang H-S, Cha D-H, Lee D-K (2005) Evaluation of the mesoscale model/land surface model (MM5/LSM) coupled model for East Asian summer monsoon simulations. J Geophys Res 110:D10105. https://doi.org/10.1029/2004JD005266
- Kiehl JT, Hack JJ, Bonan GB, Boville BA, Briegleb BP, Williamson DL, Rasch PJ, 1996: Description of the NCAR Community Climate Model (CCM3). NCAR Tech, Boulder. 143 pp
- Kumar SV, Reichle RH, Peters-Lidard CD, Koster RD, Zhan X, Crow WT, Eylander JB, Houser PR (2008) A land surface data assimilation framework using the land information system: description and applications. Adv Water Resour 31:1419–1432
- Lee JW, Hong SY, Chang EC, Suh MS, Kang HS (2014) Assessment of future climate change over East Asia due to the RCP scenarios downscaled by GRIMs-RMP. Clim Dyn 42(3–4):733–747
- Li W, Guo W, Xue Y, Fu C, Qiu B (2015) Sensitivity of a regional climate model to land surface parameterization schemes for East Asian summer monsoon simulation. Clim Dyn. https://doi. org/10.1007/s00382-015-2964-8
- Li Q, Wang S, Lee D-K, Tang J, Niu X, Hui P, Gutowski WJ Jr, Dairaku K, McGregor JL, Katzfey J, Gao X, Wu J, Hong S-Y, Wang Y, Sasaki H (2016) Building Asian climate change scenario by multi-regional climate models ensemble. Part II: mean precipitation. Int J Climatol 36:4253–4264
- Liang X-Z, Zhang F (2013) The Cloud-Aerosol-Radiation (CAR) ensemble modeling system. Atmos Chem Phys 13:8335–8364
- Liang X-Z, Kunkel KE, Samel AN (2001) Development of a regional climate model for US Midwest applications. Part 1: Sensitivity to buffer zone treatment. J Clim 14:4363–4378
- Liang X-Z, Li L, Dai A, Kunkel KE (2004a) Regional climate model simulation of summer precipitation diurnal cycle over the United States. Geophys Res Lett 31:L24208. https://doi. org/10.1029/2004GL021054
- Liang X-Z, Li L, Kunkel KE, Ting M, Wang JXL (2004b) Regional climate model simulation of US precipitation during 1982–2002. Part 1: Annual cycle. J Clim 17:3510–3528
- Liang X-Z, Choi H, Kunkel KE, Dai Y, Joseph E, Wang JXL, Kumar P (2005a) Surface boundary conditions for mesoscale regional climate models. Earth Interact 9:1–28
- Liang X-Z, Xu M, Gao W, Kunkel KE, Slusser J, Dai Y, Min Q, Houser PR, Rodell M, Schaaf CB, Gao F (2005b) Development of land surface albedo parameterization bases on Moderate Resolution Imaging Spectroradiometer (MODIS) data. J Geophys Res 110:D11107. https://doi.org/10.1029/2004JD005579
- Liang X-Z, Xu M, Choi HI, Kunkel KE, Rontu L, Geleyn J-F, Müller MD, Joseph E, Wang JXL (2006) Development of the regional Climate-Weather Research and Forecasting model (CWRF): Treatment of subgrid topography effects. In: Proceedings of the 7th Annual WRF User's Workshop, Boulder, CO, June 19–22, 5 pp

- Liang X-Z, Xu M, Kunkel KE, Grell GA, Kain J (2007) Regional climate model simulation of U.S.-Mexico summer precipitation using the optimal ensemble of two cumulus parameterizations. J Clim 20:5201–5207
- Liang X-Z, Xu M, Yuan X, Ling T, Choi HI, Zhang F, Chen L, Liu S, Su S, Qiao F, He Y, Wang JXL, Kunkel KE, Gao W, Joseph E, Morris V, Yu T-W, Dudhia J, Michalakes J (2012) Regional Climate-weather research and forecasting model (CWRF). Bull Am Meteorol Soc 93:1363–1387
- Ling T-J,X-Z, Liang M, Xu Z, Wang, Wang B (2011) A multilevel ocean mixed-layer model for 2-dimension applications. Acta Oceanol Sin 33(03):1–10
- Ling T-J, Xu M, Liang X-Z, Wang JXL, Noh Y (2015) A multi-level ocean mixed layer model resolving the diurnal cycle: development and validation. J Adv Model Earth Syst 7:1680–1692
- Liu S, Liang X-Z, Gao W, Zhang H (2008) Climate-weather research and forecasting model (CWRF) application in China: domain optimization. Chinese J Atmos Sci 32:457–468
- Liu S, Gao W, Xu M, Wang X, Liang X-Z (2009) Regional climate model simulation of China summer precipitation using an optimal ensemble of cumulus parameterization schemes. Front Earth Sci 3(2):248–257. https://doi.org/10.1007/s11707-009-0022-8
- Liu S, Liang X-Z, Gao W, He Y, Ling T (2011) Regional climate model simulations of the 1998 summer China flood: Dependence on initial and lateral boundary conditions. Open Atmos Sci J 5:96–105
- Liu S, Gao W, Liang X-Z (2013) A regional climate model downscaling projection of China future climate change. Clim Dyn 41:1871–1884. https://doi.org/10.1007/s00382-012-1632-5
- Liu D, Wang G, Mei R, Yu Z, Gu H (2014) Diagnosing the strength of land–atmosphere coupling at subseasonal to seasonal time scales in Asia. J Hydrometeorol 15:320–339
- Liu S, Wang JXL, Liang X-Z, Morris V, Fine SS (2016) A hybrid approach to improve US seasonal climate outlook skills at the regional scale. Clim Dyn 46:483–494
- Ma JH, Wang HJ, Fan K (2015) Dynamic downscaling of summer precipitation prediction over China in 1998 using WRF and CCSM4. Adv Atmos Sci 32(5):577–584
- Marcella MP, Eltahir EAB (2012) Modeling the summertime climate of Southwest Asia: The role of land surface processes in shaping the climate of semiarid regions. J Clim 25:704–719
- Mearns LO, Arritt RW, Biner S, Bukovsky M, McGinnis S, Sain S, Caya D, Correia J, Flori D, Gutowski WJ, Takle ES, Jones R, Leung R, Moufouma-Okia W, McDaniel L, Nunes AMB, Qian Y, Roads JO, Sloan L, Snyder M (2012) The North American Regional Climate Change Assessment Program: Overview of phase I results. Bull Am Meteorol Soc 93:1337–1362
- Nikulin G, Jones C, Giorgi F, Asrar G, Büchner M, Cerezo-Mota R, Christensen OB, Déqué M, Fernandez J, Hänsler A, van Meijgaard E, Samuelsson P, Sylla MB, Sushama L (2012) Precipitation climatology in an ensemble of CORDEX-Africa regional climate simulations. J Clim 25:6057–6078
- Niu X, Wang S, Tang J, Lee D-K, Gao X, Wu J, Hong S, Gutowski WJ, McGregor J (2015) Multimodel ensemble projection of precipitation in eastern China under A1B emission scenario. J Geophys Res Atmos 120:9965–9980
- Oh S-G, Park J-H, Lee S-H, Suh M-S (2014) Assessment of the RegCM4 over East Asia and future precipitation change adapted to the RCP scenarios. J Geophys Res Atmos 119:2913–2927. https://doi.org/10.1002/2013JD020693
- Oleson KW, Lawrence DM, Bonan GB, Drewniak B, Huang M, Koven CD, Levis S, Li F, Riley WJ, Subin ZM, Swenson SC, Thornton PE, Bozbiyik A, Fisher R, Heald CL, Kluzek E, Lamarque J-F, Lawrence PJ, Leung LR, Lipscomb W, Muszala S, Ricciuto DM, Sacks W, Sun Y, Tang J, Yang Z-L (2013) Improvements to the community land model and their impact on the hydrological



- cycle. NCAR Technical Note, Boulder, (NCAR/TN-503 + STR), 420p
- Pal JS, Small EE, Eltahir EAB (2000) Simulation of regional-scale water and energy budgets: Representation of subgrid cloud and precipitation processes within RegCM. J Geophy Res 105:29579–29594
- Pal JS, Giorgi F, Bi X, Elguindi N, Solmon F, Gao X, Rauscher SA, Francisco R, Zakey A, Winter J, Ashfaq M, Syed FS, Bell JL, Diffenbaugh NS, Karmacharya J, Konaré A, Martinez D, da Rocha RO, Sloan LC, Steinerand AL (2007) Regional climate modeling for the developing world: the ICTP RegCM3 and RegCNET. Bull Am Meteorol Soc 88:1395–1409
- Park S, Bretherton CS (2009) The University of Washington shallow convection and moist turbulence schemes and their impact on climate simulations with the Community Atmosphere Model. J Climate 22:3449–3469
- Qiao F, Liang X-Z (2015) Effects of cumulus parameterizations on predictions of summer flood in the Central United States. Clim Dyn 45:727–744
- Qiao F, Liang X-Z, 2016a: Effects of cumulus parameterization closures on summer precipitation simulation over the United States coastal oceans. J Adv Model Earth Syst, https://doi. org/10.1002/2015MS000621
- Qiao F, Liang X-Z (2016b) Effects of cumulus parameterization closures on simulations of summer precipitation over the continental United States. Clim Dyn. https://doi.org/10.1007/s0038 2-016-3338-6
- Reynolds RW, Smith TM, Liu C, Chelton DB, Casey KS, Schlax MG (2007) Daily high-resolution-blended analyses for sea surface temperature. J Clim 20:5473–5496
- Rinke A, Dethloff K, Cassano JJ, Christensen JH, Curry JA, Du P, Girard E, Haugen J-E, Jacob D, Jones CG, Itzow MK, Laprise R, Lynch AH, Pfeifer S, Serreze MC, Shaw MJ, Tjernström M, Wyser K, Žagar M (2006) Evaluation of an ensemble of Arctic regional climate models: Spatiotemporal fields during the SHEBA year. Clim Dyn 26:459–472
- Roads J, Chen S, Cocke S, Druyan L, Fulakeza M, LaRow T, Lonergan P, Qian J-H, Zebiak S (2003) International Research Institute/ Applied Research Centers (IRI/ARCs) regional model intercomparison over South America. J Geophys Res 108(D14):4425. https://doi.org/10.1029/2002JD003201
- Rontu L (2006) A study on parameterization of orography-related momentum fluxes in a synoptic-scale NWP model. Tellus 58:69–81
- Sato T, Xue Y (2013) Validating a regional climate model's downscaling ability for East Asian summer monsoonal interannual variability. Clim Dyn 41:2411–2426
- Shi Y, Gao XJ, Wang YG et al (2009) Simulation and projection of monsoon rainfall and rain patterns over eastern China under global warming by RegCM3. Atmos Oceanic Sci Lett 2:308–313
- Shi PJ, Sun S, Wang M, Li N, Wang JA, Jin YY, Gu XT, Yin WX (2014) Climate change regionalization in China (1961–2010). Sci China: Earth Sci 44(10):2294–2306. https://doi.org/10.1007/s11430-014-4889-1 (in Chinese)
- Skamarock WC, Klemp JB, Dudhia J, Gill DO, Barker DM, Duda MG, Huang X-Y, Wang W, Powers JG (2008) A Description of the Advanced Research WRF Version 3. NCAR Technical, Boulder, (Note, NCAR/TN-475 + STR), 113 pp
- Subin ZM, Riley WJ, Mironov D (2012) Improved lake model for climate simulations. J Adv Model Earth Syst 4:M02001. https://doi.org/10.1029/2011MS000072
- Sun Y, Solomon S, Dai A, Portmann RW (2006) How Often Does It Rain? J Climate 19:916–934
- Tang J, Li Q, Wang S, Lee DK, Hui P, Niu X, Gutowski WJ, Dairaku K, Mcgregor J, Katzfey J (2016) Building Asian climate change

- scenario by multi-regional climate models ensemble. Part I: surface air temperature. Int J Climatol 36:4241–4252
- Tao W-K, Simpson J, Baker D, Braun S, Chou M-D, Ferrier B, Johnson D, Khain A, Lang S, Lynn B, Shie C-L, Starr D, Sui C-H, Wang Y, Wetzel P (2003) Microphysics, radiation and surface processes in the Goddard Cumulus Ensemble (GCE) model. Meteor Atmos Phys, 82, 97–137
- Taylor KE (2001) Summarizing multiple aspects of model performance in a single diagram. J Geophys Res 106:7183–7192
- Tiedtke M (1989) A comprehensive mass flux scheme for cumulus parameterization in large-scale models. Mon Wea Rev 117:1779–1800
- Trenberth KE, Shea DJ (2005) Relationships between precipitation and surface temperature. Geophys Res Lett 32:L14703. https://doi.org/10.1029/2005GL022760
- Wang Y, Sen OL, Wang B (2003) A highly resolved regional climate model (IPRC-RegCM) and its simulation of the 1998 severe precipitation event over China. Part I: Model description and verification of simulation. J Climate 16:1721–1738
- Wang D, Menz C, Simon T, Simmer C, Ohlwein C (2013) Regional dynamical downscaling with CCLM over East Asia. Meteorol Atmos Phys 121(1–2):39–53
- Wang X, Tang J, Niu X, Wang S (2015) An assessment of precipitation and surface air temperature over China by regional climate models. Front Earth Sci. https://doi.org/10.1007/s11707-015-0548-x
- Wu J, Gao X-J (2013) a gridded daily observation dataset over China region and comparison with the other datasets. Chinese J Geophys 56(4):1102–1111. https://doi.org/10.6038/cjg20130406
- Wu J, Gao X-J, Xu Y-L, Pan J (2015) Regional climate change and uncertainty analysis based on four regional climate model simulations over China. Atmos Oceanic Sci Lett 8(3):147–152
- Wu F-T, Wang S-Y, Fu C-B, Qian Y, Gao Y, Lee D-K, Cha D-H, Tang J-P, Hong S-Y (2016) Evaluation and projection of summer extreme precipitation over East Asia in the Regional Model Inter-comparison Project. Clim Res 69:45–58
- Xu K-M, Randall DA (1996) A semiempirical cloudiness parameterization for use in climate models. J Atmos Sci 53:3084–3102
- Xu M, Liang X-Z, Samel A, Gao W (2014) MODIS consistent vegetation parameter specifications and their impacts on regional climate simulations. J Climate 27:8578–8596
- Xue Y, Janjic Z, Dudhia J, Vasic R, De Sales F (2014) A review on regional dynamical downscaling in intraseasonal to seasonal simulation/prediction and major factors that affect downscaling ability. Atmos Res 147–148:68–85
- Yang H, Wang B, Wang B (2012) Reduction of systematic biases in regional climate downscaling through ensemble forcing. Clim Dvn 38:655–665
- Yang H, Jiang Z, Li L (2016) Biases and improvements in three dynamical downscaling climate simulations over China. Clim Dyn. https://doi.org/10.1007/s00382-016-3023-9
- Yu ET, Wang HJ, Sun JQ (2010) A quick report on a dynamical downscaling simulation over China using the nested model. Atmos Oceanic Sci Lett 3:325–329
- Yu ET, Sun J, Chen H, Xiang W (2015) Evaluation of a high-resolution historical simulation over China: climatology and extremes. Clim Dyn 45:2013–2031
- Yuan X, Liang X-Z (2011a) Evaluation of a Conjunctive Surface-Subsurface Process model (CCSP) over the contiguous United States at regional–local scales. J Hydrometeorology 12:579–599
- Yuan X, Liang X-Z (2011b) Improving cold season precipitation prediction by the nested CWRF-CFS system. Geophys Res Lett 38:L02706. https://doi.org/10.1029/2010GL046104
- Yuan X, Liang X-Z, Wood EF (2012) WRF ensemble downscaling seasonal forecasts of China winter precipitation during 1982–2008. Clim Dyn 39:2041–2058



- Zeng X, Zhao M, Dickinson RE (1998) Intercomparison of bulk aerodynamic algorithms for the computation of sea surface fluxes using TOGA COARE and TAO data. J Climate 11:2628–2644
- Zeng M-J, Lu W-S, Liang X-Z, Wang X-L (2008) Ensemble forecast experiment on precipitation in summer by CWRF numeric model. Plateau Meteorology 27(6):1–11
- Zeng X-M, Wang M, Zhang Y, Wang Y, Zheng Y (2016) Assessing the effects of spatial resolution on regional climate model simulated summer temperature and precipitation in China: A case study. Adv Meteorol 7639567:12
- Zhang Y, Xu Y, Dong W, Cao L, Sparrow M (2006) A future climate scenario of regional changes in extreme climate events over China using the PRECIS climate model. Geophys Res Lett 33:L24702. https://doi.org/10.1029/2006GL027229
- Zhang F, Liang X-Z, Li J, Zeng Q (2013) Dominant roles of subgridscale cloud structures in model diversity of cloud radiative effects. J Geophys Res 118:7733–7749
- Zhao DM (2012) Performance of regional integrated environment modeling system (RIEMS) in the simulation of surface air temperature over East Asia. Atmos Ocean Sci Lett 5:145–150
- Zhao DM (2013) Performance of regional integrated environment modeling system (RIEMS) in precipitation simulations over East Asia. Clim Dyn 40(7–8):1767–1787
- Zhao G, Girolamo LD, Dey S, Jones AL, Bull M (2009) Examination of direct cumulus contamination on MISR-retrieved aerosol optical depth and angstrom coefficient over ocean. Geophys Res Lett 36:L13811. https://doi.org/10.1029/2009GL038549
- Zheng JY, Bian JJ, Ge QS, Hao ZX, Yin YH, Liao YM (2013) The climate regionalization in China for 1981–2010 (in Chinese). Chin Sci Bull 58:3088–3099. https://doi.org/10.1360/972012-1491

- Zhu J, Huang D-Q, Yan P-W, Huang Y, Kuang X-Y (2016) Can reanalysis datasets describe the persistent temperature and precipitation extremes over China? Theor Appl Climatol. https://doi.org/10.1007/s00704-016-1912-9
- Zou LW, Zhou TJ (2011) Sensitivity of a regional ocean-atmosphere coupled model to convection parameterization over western North Pacific. J Geophys Res 116:D18106. https://doi.org/10.1029/2011JD015844
- Zou LW, Zhou TJ (2013a) Near future (2016-40) summer precipitation changes over China as projected by a regional climate model (RCM) under the RCP8.5 emissions scenario: Comparison between RCM downscaling and the driving GCM. Adv Atmos Sci 30(3):806–818
- Zou LW, Zhou TJ (2013b) Can a regional ocean–atmosphere coupled model improve the simulation of the interannual variability of the western North Pacific summer monsoon? Adv Atmos Sci 30(3):806–818
- Zou LW, Zhou TJ, Li L, Zhang J (2010) East China summer rainfall variability of 1958–2000: Dynamical downscaling with a variable-resolution AGCM. J Clim 23:6394–6408
- Zou LW, Qian Y, Zhou TJ, Yang B (2014) Parameter tuning and calibration of RegCM3 with MIT–Emanuel cumulus parameterization scheme over CORDEX East Asia domain. J Climate 27:7687–7701
- Zou LW, Zhou TJ, Peng D (2016) Dynamical downscaling of historical climate over CORDEX East Asia domain: A comparison of regional ocean-atmosphere coupled model to standalone RCM simulations. J Geophys Res 121:1442–1458

